Acknowlegments

First and foremost, praises and thanks to Allah, the Almighty, for his conciliation in the completion of this humble work.

We are sincerely obliged to many worthy persons, without whom we could have never had the opportunity of learning greatly with interest. Special gratitude goes to our enthusiastic supervisor **Dr.A.AMMAR**, whose guidance has been present every step of our final project study. Who have always been our motivation for carrying out this work, which could not have been completed without him.

Special thanks to **Mr.H.MANSOURI**, Without his assistance and dedicated involvement in every step throughout the process, this thesis would have never been accomplished.

Pr.A.KHALDOUN, his vision,consultation, and motivation have deeply inspired us. We want to thank also **Dr.A.DRAOUI** who always guide us to complete this project.Last but not least, special thanks to **Dr.H.BELMADANI** for his kindness and help whenever needed.

Dedication

I would to dedicate this work to Allah, my Creator. My family, My beloved brothers and sisters; particularly my dearest brother, ***Aymen****, who stands by me when things look bleak , My Beautiful sisters:****Amira****,* ***Bouthaina*** *and* ***Rahma*** *who were always my source joy and delight. My dear father, who has been my most passionate fan and provided with all the materialistic and nonmaterialistic support i needed in order to finish my project in the best conditions possible, and my beloved mother who for months past, has encouraged me attentively with her fullest and truest attention and accompanied me with graceful prays throughout my whole academic journey. A special feeling of gratitude to my friend* ***MANSOURI Houssam*** *who guided me in this project step by step with his unending warm patience,* ***BENRABEH Hamza*** *who provided the all important first push through his bright mind and brilliant ideas which gave me the inspiration required to start this project,****BOUKHDICHE Taieb*** *whose words of encouragement and emotional support lit fire into my soul and filled passion into my heart, thank you your encouragement have carried me over many hardships, i also would like to send the warmest of greeting to my friend* ***KEROUCHE Yassmina*** *for providing me with her personal Laptop without her endless generosity this work would have never been done in the first place,thanx to* ***BENSALLEH Takwa*** *for helping me in writing this thesis without forgeting* ***BASIR Romaissa****,who always have been by my side. A very special thank you to* ***TAIB Amine*** *who at the times i felt lost in this project and struggled to find a way out, when everything was dark and i felt like giving up, he was there to give me a warm helping hand and a bright guiding light that showed me the way throughout the darkest of moments. Thank you* ***BOUZENZEN Rawneq*** *for always being there for me through the bad times and the good,i'm so appreciative of all that you do for me. Last but not least,thank you* ***ROUBACHE Karima****,my partner in this project,for being one of the most incredible friends anyone ever could ask for,please know that i'm so grateful to have you in my life.*

BOUARADA Meriem

Dedication

This work is wholeheartedly dedicated to: Allah, my Creator and my Master, My great teacher and messenger, Mohammed (May Allah bless and grant him). My beloved parents, who have been my source of inspiration and gave me strength when I thought of giving up, who continually provide their moral, spiritual, emotional, and financial support. My love for you can never be quantified. Thank you. My faithful brother,Who have always helped me and believed that I could do it.My lovely and supportive neighbor, who has been a constant source of support and encouragement during the challenges of graduation and life. I am truly thankful for having you by my side.All my family and my dear friends whoever helped to achieve this work.My dear partner Meriem, for being an amazing companion during this journey.

ROUBACHE Karima

Abstract

Several research works have been pushed by industry to develop electric vehicles. This study aims at optimizing the cost and energy of the electric powertrain that is based on two induction motors supplied by two independent inverters in the conventional case, but this solution is expensive in terms of size and number of power switches. Thanks to its special topology with reduced number of semiconductor switches, the nine switch inverter has been suggested as a substitution to two conventional two level inverters. On the other hand, thanks to the robustness of direct torque control scheme as compared to other vector control methods, (DTC) proves to be a well suited control scheme for electric vehicle applications. Nowadays, the brilliant technology in automotive industry towards regenerative braking is improving, thus bidirectional DC-DC converters are used for capturing the kinetic energy of motor and charging the battery during regenerative mode.

In this context, a control of an electric vehicle traction chain based on dual induction motor drive using nine switch inverter is investigated in this report, to study the independency control of nine switch inverter powered motors. Furthermore, the effectiveness of the developed controllers in separating between the flux and torque control have been checked. Likewise, the regenerative braking has been studied to promote the efficiency and realization of energy saving in the electric vehicles.

Simulation of these techniques were then carried out using MATLAB/Simulink software and the obtained results analyzed and discussed to confirm the validity of the proposed techniques.

Contents

List of Figures

List of Tables

Abbreviations

EV: Electric Vehicle.

ICEV: Internal Combustion Engine Vehicle.

VSI: Voltage Source Inverter.

BEV: Battery Electric Vehicle.

PHEV: Plug-in Hybrid Electric Vehicle.

HEV: Hybrid Electric Vehicle.

FCEV: Fuel Cell Electric Vehicle.

EREV: Extended Range Electric Vehicle.

NEDC: New European Driving Cycle.

FTP: Federal Test Procedure.

AC: Alternative Current.

DC: Direct Current.

IM: Induction Motor.

EMF: Electro-Motive Force.

NSI: Nine Switch Inverter.

XOR: logic operation gate Exclusive OR.

DTC: Direct Torque Control.

PI: Proportional-Integral.

IGBT: Insulated Gate Bipolar Transistor.

FOC: Field Oriented Control.

VFD: Variable Frequency Drive.

PWM: Pulse Width Modulation.

GTO: Gate Turn-Off Thyristor.

MOSFET: Metal Oxide Semiconductor Field Effect Transistor.

IGCT: Integrated Gate Commutated Thyristor.

DSC: Direct Self Control.

SPWM: Sinusoidal Pulse Width Modulation.

PID: Proportional Integral Derivative.

SOC: State Of Charge.

General introduction

The development of internal combustion engine automobiles is one of the greatest achievements of modern technology. However, the highly developed automotive industry and the increasingly large number of automobiles in use around the world are causing serious problems for the environment and hydrocarbon resources. The deteriorating air quality, global warming issues, and depleting petroleum resources are becoming serious threats to modern life. Progressively more rigorous emissions and fuel efficiency standards are stimulating the aggressive development of safer, cleaner, and more efficient vehicles. It is now well recognized that electric, hybrid electric, and fuel-cell vehicles are a promising technology for achieving a sustainable transport sector in the future, due to their very low to zero carbon emissions, low noise, high efficiency, and flexibility in grid operation and integration.

This report deals with a Direct Torque Control for Nine Switches Inverter fed two induction motors-based electric vehicles (EVs). In the electric vehicle motorization, induction motors are widely used due to their convenience in terms of robustness, compactness, reliability and cost. In the conventional case, the traction is based on two induction motors supplied by two independent inverters. Regarding size and the quantity of power switches, this approach is pricey. Finding and proving a novel design for the vehicle's traction using a single converter is the aim of this project, which will decrease the total number of components (only nine switches instead of twelve), simplify the entire system, and lower system losses.

For the nine switches inverter (NSI), a pulse width modulation PWM switching sequence control technique was applied. This technique provides open loop control of the inverter which has low accuracy. To control the NSI in closed loop, DTC will be chosen due to its advantages in terms of robustness against parameters variation, its easy implementation, fast dynamic responses and it provides independent control of two driving wheels. In addition, this structure offers the possibility to eliminate the mechanical differential and replacing it with a software differential (synchronization). Synchronism between the two motors is used to ensure the stability for the vehicle when cornering or under slippery road conditions.

In the battery part, two types of unidirectional DC-DC converter will be integrated to boost the voltage of the battery to such level where it can supply both motor. One of the most important features of EVs, is their ability to recover significant amounts of braking energy. The electric motors in EVs, can be controlled to operate as generators to convert the kinetic or potential energy of vehicle mass into electric energy that can be stored in the energy storage and then reused. Bidirectional buck boost converter is used for the regenerative braking. Hence, different concepts will be discussed and several simulations will be conducted.

Organization of the report:

Chapter one includes back ground and generalities on electric vehicles from history to the different types of existing electric vehicles. Also, different types of electric motors used to drive the traction chain. EVs taxonomy and traction chain were discussed.

Chapter two deals with the modelling and description of IM and how to control it using variable speed drive. It also presents the NSI, principle of operation and PWM technique used and we end up this chapter with simulation which ensures the validity of NSI's outputs.

Chapter three describes basic principle of operation of DTC, and estimation and control of both flux and torque and ending up this chapter with simulation, which insures the validity of DTC.

Chapter four is aimed at DTC method used for two induction motors fed by NSI with simulation results followed by discussion. Also, it handles the battery part, its charging and discharging mechanism.

Finally, a general conclusion of this work and perspectives are listed at the end.

Chapter 1

Generalities about electric vehicles

1.1 Introduction

In a world where environment protection and energy conservation are growing concerns, the development of electric vehicles (EVs) has taken on an accelerated pace. In fact, the development of numerous types of electric vehicles is a result of the revolution in drivetrain technology. Depending on their purpose and design, today's electric vehicles can be powered by a single source or a combination of several.

1.2 Brief history

EVs are nothing new, they were invented 178 years ago but lost the competition for dominance to internal combustion engine vehicles (ICEVs). Actually, the first EV was a battery powered tricycle built by Thomas Davenport in 1834, (Figure1-1). In 1900, among an annual sale of 4200 automobiles in the US, 38% were EVs, 22% ICEVs, and 40% steam powered vehicles. At that time, EVs were the preferred road transportation among the wealthy elite, their cost was equivalent to a Rolls Royce of today. A man with an idea that finished off the EVs for good was Ford. His mass produced Ford Model T could offer a range double or triple that of the EVs but at only a fraction of their cost. By the 1930s, the EVs almost vanished from the scene. The rekindling of interests in EVs started at the outbreak of the energy crisis and oil shortage in the 1970s. Owing to the growing concern over air quality and the possible consequences of the greenhouse effect in the 1980s, the pace of EV development was accelerated[1].

Figure 1-1: The first EV made by Thomas Danverport in 1834 [1].

1.3 General description of traction chain

EVs traction chain consists of four main components : the electric motor, voltage source inverter, DC-DC converter and battery pack.

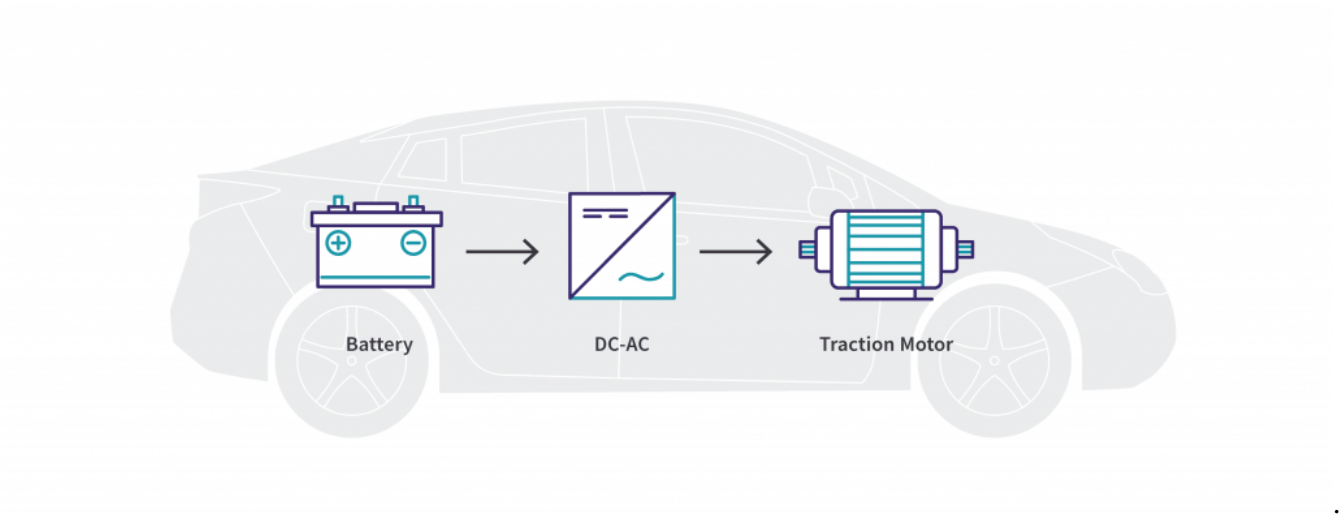

Figure 1-2: Traction chain of an electric vehicle.

1.3.1 Electric motor

The main component of an electric vehicle that transforms the electrical energy from the battery into rotation that can be used to move the vehicle.

Most used motor types in EVs

There are various types of motors used for EVs. This project is going to investigate IM. Table 1.1 illustrates a comparison between the most used motor types in EV.

Table 1.1: Comparison between most used motor types in EV[4][5].

Motor Type	Advantages	Disadvantages	Vehicles Used In
Brushed DC Motor	• Maximum torque at low speed	• Bulky structure • Low efficiency • Heat generation at brushes	Fiat Panda Elettra , ConceptorG-Van.
Permanent Magnet Brushless DC Motor(BLDC)	• No rotor copper losses • High efficiency	• Short constant power range • Decreased torque with increase in speed • High cost because of PM	Toyota Prius (2005)
Permanent Magnet Synchronous Motor(PMSM)	• Efficient • Compact • High torque even at very low speeds	• Huge iron losses at high speeds during In-wheel operation	Toyota Prius, Nissan Leaf, Soul EV
Induction Motor(IM)	• Simple construction • Low cost and small size • High reliability • Simple maintenance • Robustness • Operation at different environmental conditions	• High losses • Low power factor.To overcome these problems, dual inverters are used for the purpose of extending constant power, and rotor losses are reduced in design stage	Tesla Model S,Tesla Model X, Toyota RAV4,GM EV1

In-wheel motor configutation

According to the number of motors used in the vehicle and their arrangement, different configurations are used in EVs. Our main focus will be about the In-wheel motor configuration.

In the In-wheel motor configuration, Figure1-3, instead of having a single motor placed

under the hood, two (or even four) smaller motors are inserted directly into the wheels of the vehicle. This system allows, on the one hand, to control with high precision and independently the torque applied to each wheel and, on the other hand, to maximize the capacity of the regenerative braking [7].

The use of this type of configuration on steered wheels allows the elimination of all mechanical parts linked to the transmission, to independently control the wheels and at the same time, to deliberate space in the vehicle[7].

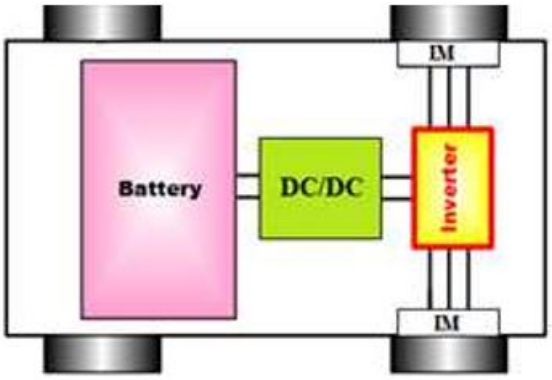

Figure 1-3: In-wheel dual motor configuration.

1.3.2 Voltage source inverter

When an EV has AC motors, the energy from the battery must be converted using VSI in order to be used. The inverter also operates when the car is using regenerative braking converting the alternating current generated by the electric motors into direct current to be stored in the battery.

This report examines the NSI topology, and more detailes will be explained in the next chapter.

1.3.3 DC-DC converter

Different configurations of EV power supply show that at least one DC-DC converter is necessary to control the DC-link [8]. A DC-DC converter is a category of power converters, which converts a DC source from one voltage level to another. It can be unidirectional, which transfers power only in one direction, or bidirectional, which can transfer power in either direction [9]. There are two types of DC-DC converters (see figure1-4), isolated and non isolated converters.

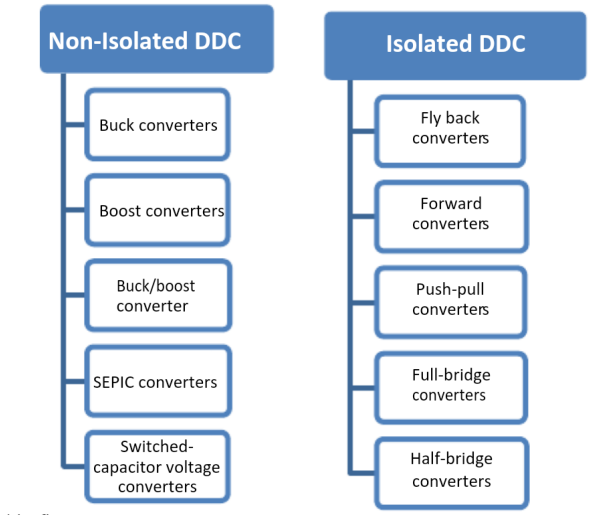

Figure 1-4: Classification of DC-DC converters[2].

1.3.4 Battery pack

It is the reservoir that contains the energy the car will use to drive, operate the heating and cooling, and run all of the other lights and accessories (see Figure1-5)
In fact, among many kinds of batteries, Lithium-ion batteries have become the focus of research interest for EVs.

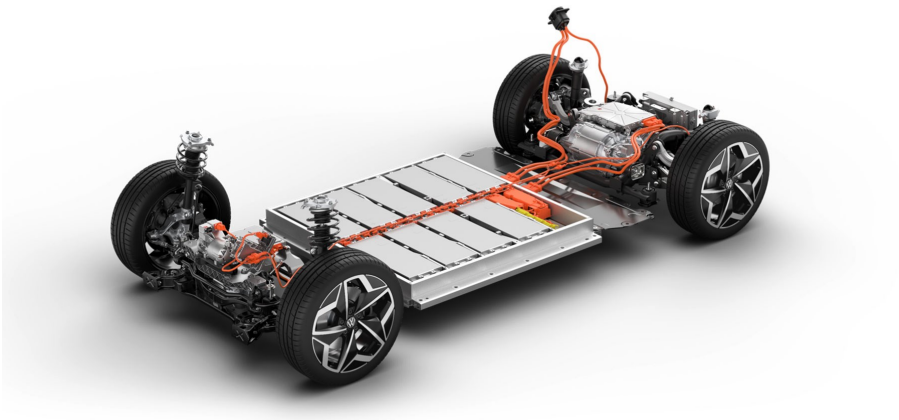

Figure 1-5: Battery pack of an EV.

Lithium-Ion batteries

A Lithium-ion (Li-ion) battery is a type of rechargeable battery used in EVs and a number of portable electronics. When compared to other batteries, lithium-ion batteries have many advantages in terms of functionality and safety, (see Table1.2).

Table 1.2: Comparison between Li-ion and different battery types[6].

Advantages Over	**Lead-Acid**	**Ni-Cd(Nickel-Cadmium)**	**NiMH(Nickel-Metal Hybride)**
Li-Ion	• Cost • Safety • Higher cyclability • Recyclability	• Range of operating temperature • Cost • Safety • Higher cyclability • Recyclability	• Cost • Safety • Rate of discharge • Recyclability

1.4 Electric vehicles taxonomy

Nowadays, we can encounter different types of EVs, according to their technology. In general, they are sorted in five types listed in Figure 1-6), with sitting some examples from the EV market:

1.4.1 Battery electric vehicles (BEVs)

Vehicles 100% are propelled by electric power. BEVs do not have an internal combustion engine and they do not use any kind of liquid fuel. BEVs normally use large packs of batteries in order to give the vehicle an acceptable autonomy. An example of this type of vehicle is the Nissan Leaf, which is 100% electric and it currently provides a $62kWh$ battery that allows users to have an autonomy of $360km$ [6].

1.4.2 Plug-In hybrid electric vehicles (PHEVs)

Hybrid vehicles are propelled by a conventional combustible engine and an electric engine charged by a pluggable external electric source. PHEVs can store enough electricity from the grid to significantly reduce their fuel consumption in regular driving conditions. The Mitsubishi Outlander PHEV provides a $12kWh$ battery, which allows it to drive around $50km$ just with the electric engine [6].

1.4.3 Hybrid electric vehicles (HEVs)

Hybrid vehicles are propelled by a combination of a conventional internal combustion engine and an electric engine. The difference with regard to PHEVs is that HEVs cannot be plugged to the grid. In fact, the battery that provides energy to the electric engine is charged thanks to the power generated by the vehicle's combustion engine. The Toyota Prius, in its hybrid model (4th generation), provided a $1.3kWh$ battery that theoretically allowed it an autonomy as far as 25 km in its all-electric mode [6].

1.4.4 Fuel cell electric vehicles (FCEVs)

These vehicles are provided with an electric engine that uses a mix of compressed hydrogen and oxygen obtained from the air, having water as the only waste resulting from this process. The Hyundai Nexo FCEV is an example of this type of vehicles, being able to travel $650km$ without refueling [6].

1.4.5 Extended-range electric vehicles(ER-EVs)

These vehicles are very similar to those ones in the BEV category. However, the ER-EVs are also provided with a supplementary combustion engine, which charges the batteries of the vehicle if needed. This type of engine, unlike those provided by PHEVs and HEVs, is only used for charging, so that it is not connected to the wheels of the vehicle. An example of this type of vehicles is the BMW i3, which has a $42.2kWh$ battery that results in a $260km$ autonomy in electric mode, and users can benefit an additional $130km$ from the extended-range mode [6].

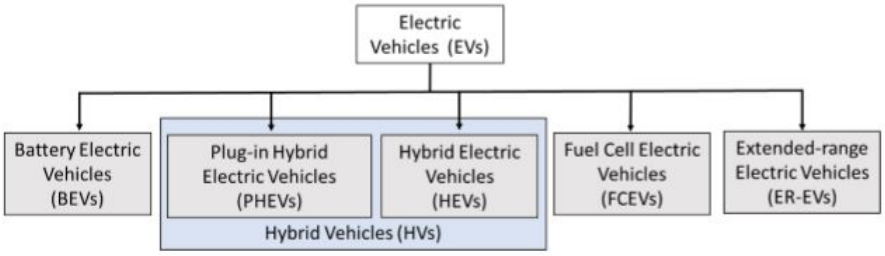

Figure 1-6: EVs classification according to their engine technologies.

1.5 Regenerative braking in electric vehicles

Regenerative braking can be used in EVs as a process for recycling the brake energy, which is impossible in the conventional internal combustion vehicles.Regenerative braking is the pro-

cess of feeding energy from the drive motor back into the battery during the braking process, when the vehicle's inertia forces the motor into generator mode. In this mode, the battery is considered as a load, thereby providing a braking force to EV[10].

In general, there are four possible modes or quadrants of operation depending on direction of rotation as shown in Figure1-7 .

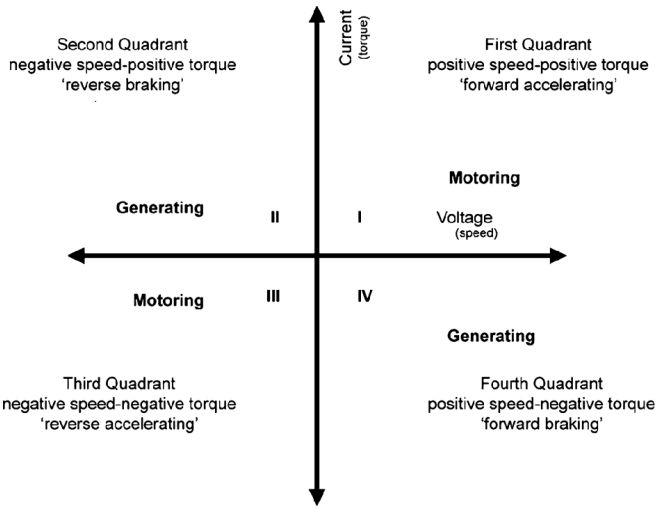

Figure 1-7: Four quadrant operation modes of the electric machine.

1.6 Advantages and disadvantages of electric vehicles

The electric vehicle has several advantages and drawbacks that are summerized in Table 1.3.

Table 1.3: Advantages and disadvantages of electric vehicles.

Advantages	**Disadvantages**
• Highly efficient • Reduced emissions • High performance and Low maintenance • Simplified power train • Very responsive and have very good torque	• The range of an electric car depends on its battery • Battery charging is time consuming • Battery repairs or replacement can be expensive • Sufficient public charging infrastructure is still lacking

1.7 Driving cycle

Driving cycle is a velocity-time profile that describes driving characteristics of specific type of vehicles under real world driving condition, which is always used as a standard for the evaluation of vehicles' economy, emission and driving range in vehicle industry[11].

Driving cycles can be classified as Model Driving Cycles and Transient Driving Cycles.

- **Model driving Cycle**

  The model driving cycle comprises constant speed and does not represent a real driving pattern of a vehicle. These driving cycles will be used for specific applications such as an emission test [12]. New European Driving Cycle (NEDC) is an example of Model Driving Cycle (see figure1-8).

- **Transient driving Cycle**

  Represents an actual pattern of a vehicle which contains acceleration, deceleration, constant speed, etc [12]. Federal Test Procedure (FTP 75) is an example of a Transient Driving Cycle.

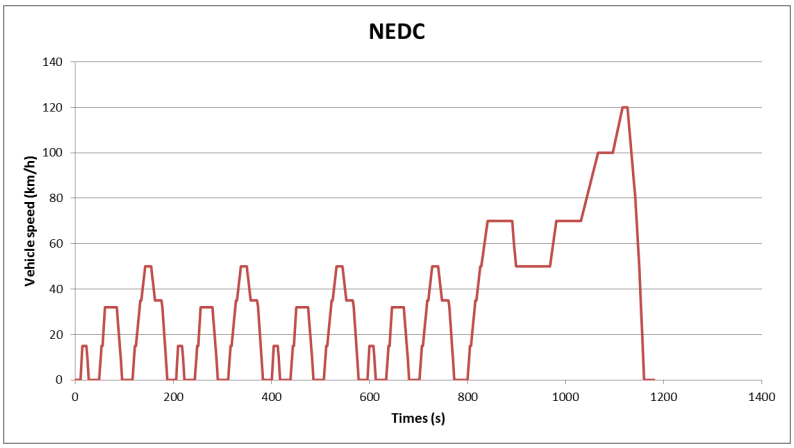

Figure 1-8: New European Driving Cycle (NEDC).

1.8 Conclusion

During this chapter, we have presented a general overview of electric vehicles (EVs), starting with exposing their evolution through time, then we gave a global description of the traction chain of the electric vehicles types, as well as their classification according to energy sources. The regenerative braking phenomena was further discussed and a synthesis on all of these, allowed us to provide a clearer vision on their advantages and disadvantages. In the next chapter, we approach the modeling of two main parts of our traction chain system:IM and NSI.

Chapter 2

Background on induction motor and drives

2.1 Introduction

Induction motors are invading into the application areas of motor drive whether being domestic application or industry due to their convenience in terms of robustness, compactness, reliability and cost. In particular, a variety of these motors are needed for factory applications, such as manipulating industrial robots. In many cases, there are two or more ac loads that require independent control. Therefore, a dual output inverter have been developed which consists of nine switches only and can drive two motor independently .

There are two methods of controlling dual IM :
providing two separate inverters to drive each motor or by connecting the two motors in parallel and using a single inverter to drive them both. The first technique complicates the process and requires large expense to be implemented. The second method cannot provide independent control of the two motors. Thus, we propose the nine switch inverter that independently controls two three-phase loads[13].

2.2 Induction motor overview

In general, Induction motor (IM) is used for converting electric energy into mechanical energy. IM was invented by Nikola Tesla in the last quarter of nineteenth century and which now is very significant in our daily life and available as single and three-phase IM. It consists of two main parts: the stator (stationary part) and the rotor (rotating part),where an alternating

current is applied to the stator to create a rotating magnetic field. The rotor, reacts with the magnetic field to rotate within the stator. Figure 2-1 represents its general structure[14].

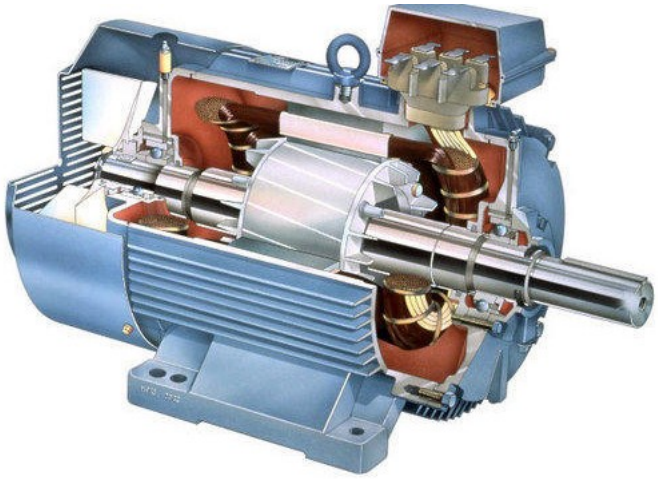

Figure 2-1: Induction Motor general structure.

2.3 Induction motor modeling

The modeling process consists of applying the electromagnetic laws to the different windings and motion equations to the rotor carrying the load[15].

2.3.1 Voltage equations

The stator and rotor voltage equations are given by the equation 2.1 and equation 2.2 :

$$[V_{sabc}] = [R_s] * [I_{sabc}] + \frac{d}{dt} * [\phi_{sabc}] \tag{2.1}$$

$$0 = [V_{rabc}] = [R_r] * [I_{rabc}] + \frac{d}{dt} * [\phi_{rabc}] \tag{2.2}$$

where:

$[V_{sabc}] = \begin{bmatrix} V_{sa} \\ V_{sb} \\ V_{sc} \end{bmatrix}$ is the vector of the stator voltages ,$[V_{rabc}] = \begin{bmatrix} V_{ra} \\ V_{rb} \\ V_{rc} \end{bmatrix}$ is the vector of the rotor voltages ,$[I_{sabc}] = \begin{bmatrix} I_{sa} \\ I_{sb} \\ I_{sc} \end{bmatrix}$ is the vector of the stator currents,$[I_{rabc}] = \begin{bmatrix} I_{ra} \\ I_{rb} \\ I_{rc} \end{bmatrix}$ is the

vector of the rotor currents, $[\phi_{sabc}] = \begin{bmatrix} \phi_{sa} \\ \phi_{sb} \\ \phi_{sc} \end{bmatrix}$ is the vector of the stator flux,

$[\phi_{rabc}] = \begin{bmatrix} \phi_{ra} \\ \phi_{rb} \\ \phi_{rc} \end{bmatrix}$ is the vector of the rotor flux,$[R_s] = \begin{bmatrix} R_s & 0 & 0 \\ 0 & R_s & 0 \\ 0 & 0 & R_s \end{bmatrix}$ and

$[R_r] = \begin{bmatrix} R_r & 0 & 0 \\ 0 & R_r & 0 \\ 0 & 0 & R_r \end{bmatrix}$ are the resistance matrices of the stator and the rotor, respectively.

2.3.2 Flux equations

Assuming a linear magnetic path, the stator and rotor flux equations can be expressed by equation 2.3 and 2.4 :

$$[\phi_{sabc}] = [L_{os}] * [I_{sabc}] + [M_{osr}] * [I_{rabc}] \tag{2.3}$$

$$[\phi_{rabc}] = [L_{or}] * [I_{rabc}] + [M_{osr}] * [I_{sabc}] \tag{2.4}$$

where :

$[L_{os}] = \begin{bmatrix} l_s & M_{os} & M_{os} \\ M_{os} & l_s & M_{os} \\ M_{os} & M_{os} & l_s \end{bmatrix}$ and $[L_{or}] = \begin{bmatrix} l_r & M_{or} & M_{or} \\ M_{or} & l_r & M_{or} \\ M_{or} & M_{or} & l_r \end{bmatrix}$ are the

inductor matrices of the stator and rotor, respectively . l_s and l_r are the self inductances, M_{os} is the mutual inductance between two stator phases and M_{or} is the mutual inductance between two rotor phases , and

$[M_{osr}] = M \begin{bmatrix} \cos(p\theta) & (\cos p\theta + \frac{2\pi}{3}) & (\cos p\theta + \frac{4\pi}{3}) \\ (\cos p\theta + \frac{4\pi}{3}) & \cos(p\theta) & (\cos p\theta + \frac{2\pi}{3}) \\ (\cos p\theta + \frac{4\pi}{3}) & (\cos p\theta + \frac{2\pi}{3}) & \cos(p\theta) \end{bmatrix}$ is the mutual

inductance matrix between the stator and the rotor. M presents the maximal mutual inductance between the stator phase and the rotor phase. p designates the number of pole pairs and θ denotes the angle between the stator and the rotor.

2.3.3 Mechanical equations

The rotor motion undergoes the following usual second order differential equation :

$$J\frac{d\omega_m}{dt} = -F\omega_m + T_{em} - T_L - T_d \tag{2.5}$$

where :

ω_m , T_L , T_{em} and T_d are, respectively, the rotor speed, the load torque, the electromagnetic motor torque, and the dry torque. J designates the inertia of the rotor-load set and F the viscous friction coefficient. The expression of T_{em} obtained from the energy balance and it's shown bellow

$$T_{em} = \frac{\partial W_{mag}}{\partial \theta} \tag{2.6}$$

with:

$$W_{mag} = \frac{1}{2}([I_{sabc}]^T * [\phi_{sabc}] + [I_{rabc}]^T * [\phi_{rabc}])$$

2.3.4 Clarke transformation

The three-phase quantities are translated from the three-phase reference frame to the two-axis orthogonal stationary reference frame using Clarke transformation as it is expressed by equation 2.7 and 2.8:

$$I_{\alpha\beta 0}(t) = TI_{abc}(t) = \sqrt{\frac{2}{3}} \begin{bmatrix} 1 & \frac{-1}{2} & \frac{-1}{2} \\ 0 & \frac{\sqrt{3}}{2} & \frac{-\sqrt{3}}{2} \\ \frac{1}{\sqrt{2}} & \frac{1}{\sqrt{2}} & \frac{1}{\sqrt{2}} \end{bmatrix} \begin{bmatrix} I_a(t) \\ I_b(t) \\ I_c(t) \end{bmatrix} \tag{2.7}$$

the inverse transformation in this case is

$$I_{abc}(t) = \sqrt{\frac{2}{3}} \begin{bmatrix} 1 & 0 & \frac{1}{\sqrt{2}} \\ \frac{-1}{2} & \frac{\sqrt{3}}{2} & \frac{1}{\sqrt{2}} \\ \frac{-1}{2} & \frac{-\sqrt{3}}{2} & \frac{1}{\sqrt{2}} \end{bmatrix} \begin{bmatrix} I_\alpha(t) \\ I_\beta(t) \\ I_0(t) \end{bmatrix} \tag{2.8}$$

where:

I_a, I_b,andI_c are three-phase quantities. I_α and I_β are stationary orthogonal reference frame quantities. Applying the Clarke transformation to the induction machine equations 2.1 and 2.2

yields to equations 2.9and 2.10:

$$[V_{s\alpha\beta}] = [R_s] * [I_{s\alpha\beta}] + \frac{d}{dt} * [\phi_{s\alpha\beta}] \tag{2.9}$$

$$0 = [V_{r\alpha\beta}] = [R_r] * [I_{r\alpha\beta}] + \frac{d}{dt} * [\phi_{r\alpha\beta}] \tag{2.10}$$

2.4 Variable frequency drives

When motors are supplied directly from the power network, the supply power frequency is constant, $(50Hz/60Hz)$.To manage the speed when necessary, additional mechanical systems are used: dampers, valves, gear boxes, brakes, etc. Mechanical systems reduce the overall system efficiency. But since the development of the power electronic converts, it can be used now in variable frequency by inserting a converter between the motor and the electrical grid. This make it possible to obtain an adjustable speed motor. VFDs control the motor speed and motor torque by controlling the frequency and magnitude of voltages and currents supplied to the motor. Each VFD has three sections: rectifier, filter with energy storage and inverter. Typical conceptual configuration is shown in Figure 2-2 [16].

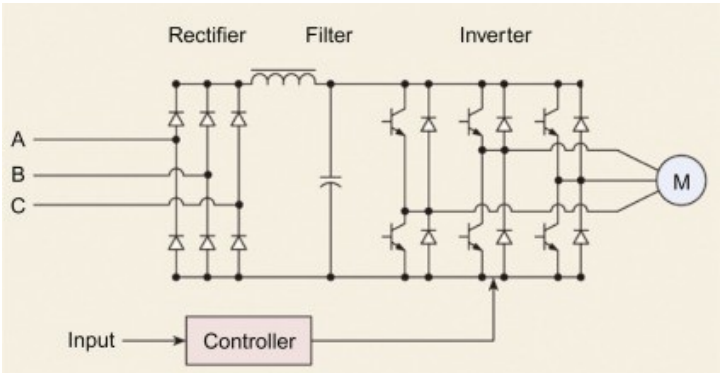

Figure 2-2: Variable frequency drive configuration.

Rectifier takes the fixed frequency and magnitude voltage sinusoidal from the grid and rectifies it into DC waveform. Filter takes the DC waveform from rectifier and provides almost pure linear DC. Energy storage is used to support instantaneous energy balance. Capacitors and inductors are used for energy storage. Inverter inverts the DC power back to AC through a set of electronic switches (MOSFET, IGBT ,IGCT ,GTO, etc.). These switches, by opening and closing at certain speeds and durations, can invert DC and recreate output currents and voltage waveforms that mimic sinusoidal AC waveforms. The motor is then supplied from the output of the inverter.

The output waveforms are pulse width modulated (PWM) waveforms. They are called PWM waveforms because they are created by multiple pulses of the switches at short intervals. The magnitude and frequency of PWM voltage waveforms are adjustable. Typical PWM waveform with sinusoid being approximated is shown in Figure 2-3 [16].

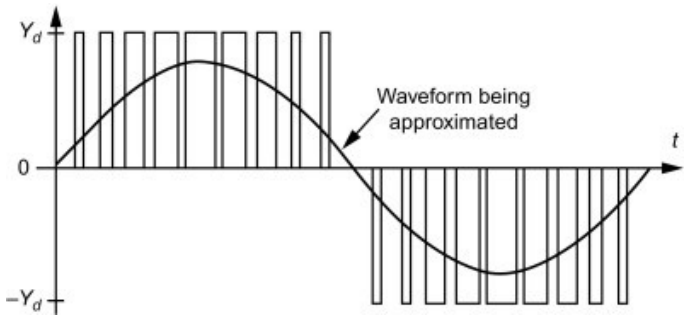

Figure 2-3: Typical PWM waveform.

The employment of the variable speed motor drive in open loop may offer a satisfied performance at steady state without need of speed regulation for simple applications. But, in cases where the drive requires fast dynamic response and accurate speed, the open loop control becomes unsatisfactory. Therefore, it is necessary to operate the motor in a closed loop mode. Several techniques have been proposed for this purpose. They are classified mainly into scalar and vector controls[15]. Figure 2-4 illustrates the different classification of the variable frequency drives control strategies.

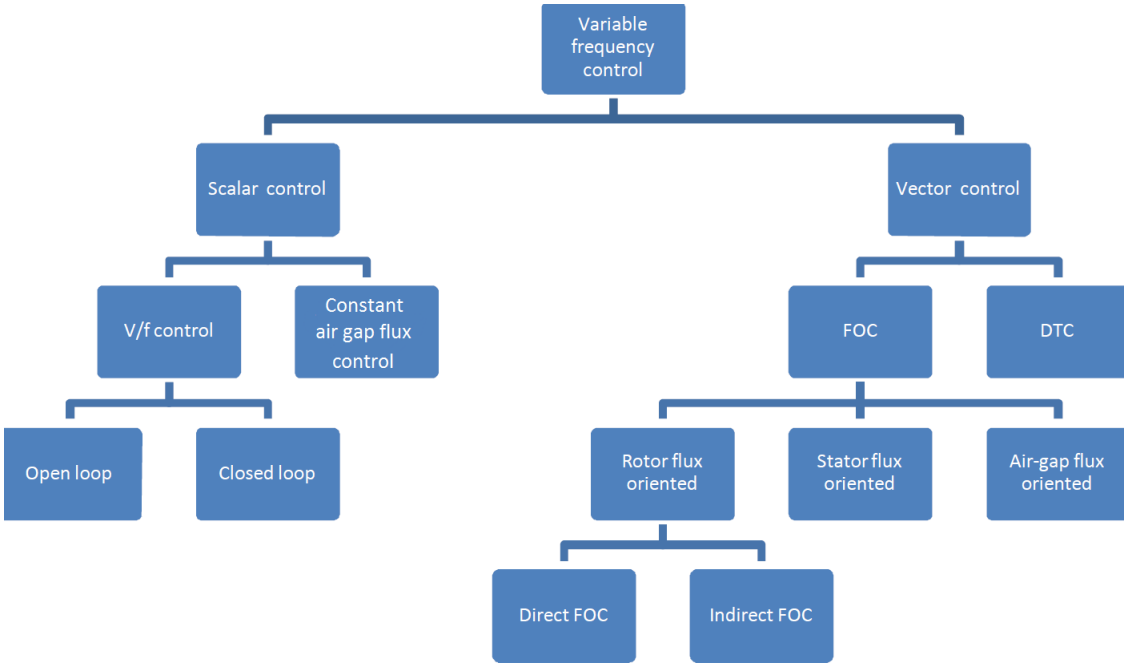

Figure 2-4: Variable frequency drives control strategies.

- **Direct Torque Control (DTC):**

Which takes the most of our interest. It was introduced by Takahashi and Nagochi in the middle of 1980s in Japan. and also in Germany by Depenbrock under the name of Direct Self-Control (DSC). In contrast to FOC, this control is completely done in stationary frame (stator fixed coordinates). Furthermore, DTC generates the inverter gating signals directly through a look up switching table and the use of modulator is not necessary. It offers an excellent torque response using less model's parameters than FOC. Due to its simplicity and very fast response, it can be so applicable for high performance drive applications. More details about it will be presented in the next chapter[15].

2.5 Voltage source inverter

Voltage source inverter (VSI) is mainly used to convert a constant DC voltage into an AC voltage with variable magnitude and frequency.

2.5.1 Six switch voltage source inverter

Figure 2-5 shows the power circuit of a three-phase voltage source inverter.

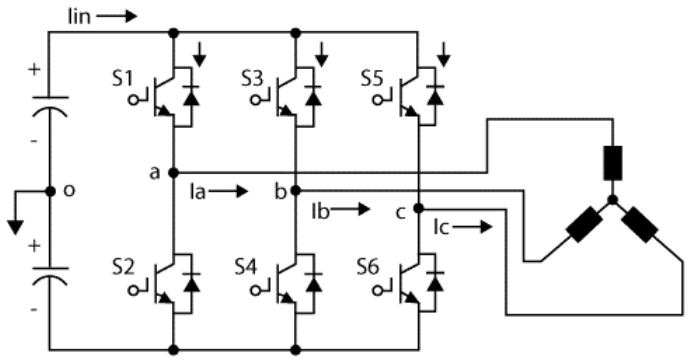

Figure 2-5: Six switch voltage source inverter.

The leg voltages are denoted by V_A,V_B,V_C where the relationship between the leg voltage and switching signals is given by :

$$V_K = (S_K - 0.5) * V_{dc} \qquad K \in (A, B, C) \tag{2.11}$$

where $S_K = 1$ when the upper power switch is 'ON' and $S_K = 0$ when the lower switch is 'ON'. To avoid shorting the DC rail, the upper and the lower switches are complimentary. The

total possible outputs are $(2^3) = 8(000, 001, 010, 011, 100, 101, 110, 111)$. Thus, there are six active switching states and two zero switching states. The space vectors are shown graphically in complex plan $\alpha\beta$ in Figure 2-6[3].

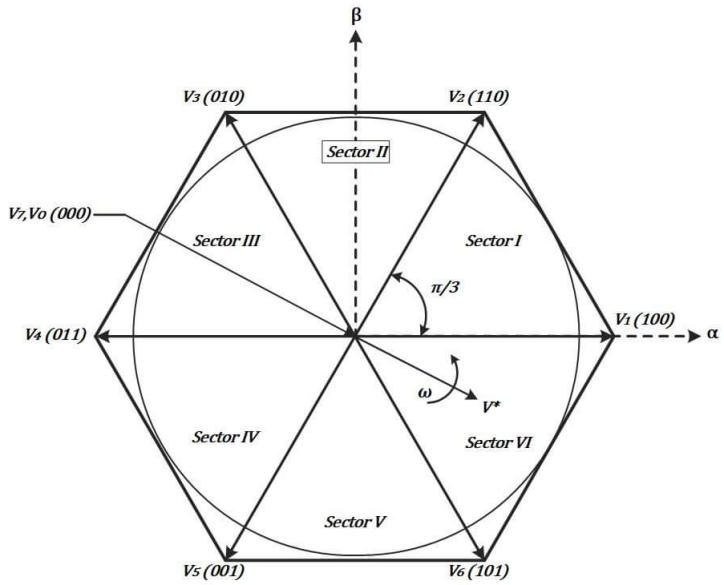

Figure 2-6: Different voltage vectors generated by a six-switch inverter.

the following expressions present a model of three-phase inverter :

$$\begin{bmatrix} V_{an} \\ V_{bn} \\ V_{cn} \end{bmatrix} = (\frac{V_{dc}}{3}) \begin{bmatrix} 2 & -1 & -1 \\ -1 & 2 & -1 \\ -1 & -1 & 2 \end{bmatrix} \begin{bmatrix} S_a \\ S_b \\ S_c \end{bmatrix} \tag{2.12}$$

In addition, any three-phase system defined by: $V_{an}(t), V_{Bn}(t), V_{Cn}(t)$can be represented uniquely by a rotating vector V_s[3]:

$$V_s = \frac{2}{3} * [v_{an} + V_{bn}exp(^i\frac{2\pi}{3}) + V_{cn}exp(^i\frac{4\pi}{3})] \tag{2.13}$$

2.5.2 Nine switch voltage source inverter

NSI is a new semiconductor-minimized topology that was first created to drive two separate motors. Comparing to the traditional two bridges configuration with total twelve switches, the NSI can save three switches easily fulfilling the practical concern of cost reduction. It has been conceived by replacing the middle six switches of the classical dual output inverter by only three switches. Both inverters are shown in Figure 2-7[17].

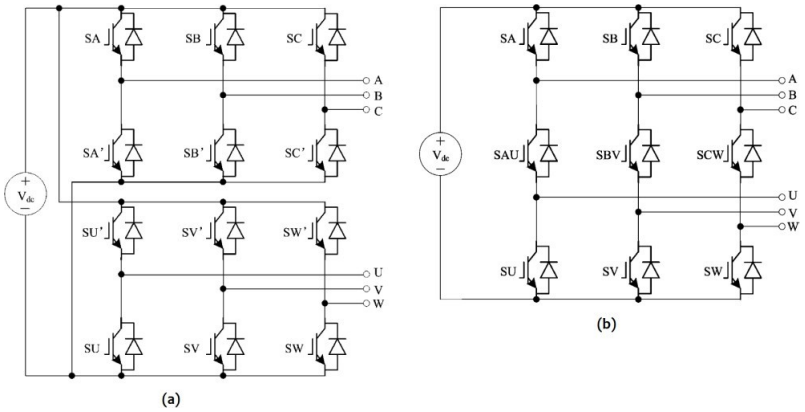

Figure 2-7: (a) The classical Dual output inverter, (b) Nine-switch inverter.

2.5.3 Sinusoidal PWM of NSI

A PWM signal is generated using two reference signals and one carrier signal in order to control the NSI as it is shown in Figure 2-8.

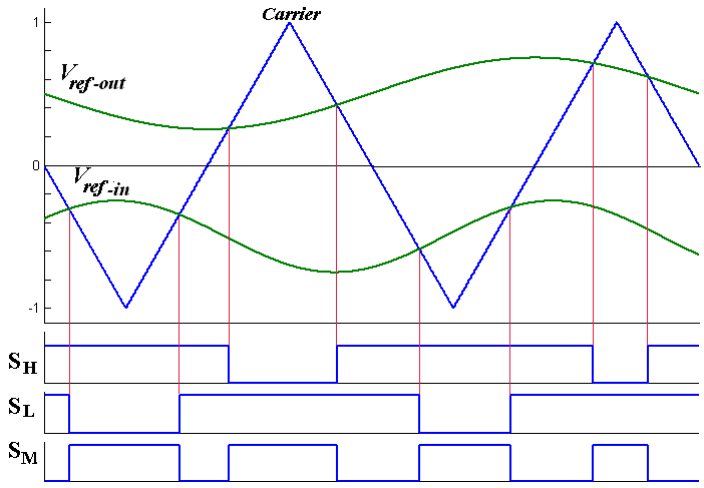

Figure 2-8: Generation of PWM signal.

For each leg, the gate signal of the upper switch is generated by comparing the upper half of a high frequency triangular carrier signal with a sinusoidal reference signal. The gate signal of the lower switch is generated by comparing the lower half of the same carrier signal with another sinusoidal reference signal. In order to avoid closing the three switches of the same leg simultaneously and therefore shorting the DC source, the gate signal of the middle switch is generated by a XOR logic gate whose inputs are the two gate signals of the upper and lower switches. Figure 2-9 bellow explains the XOR signal generation[18].

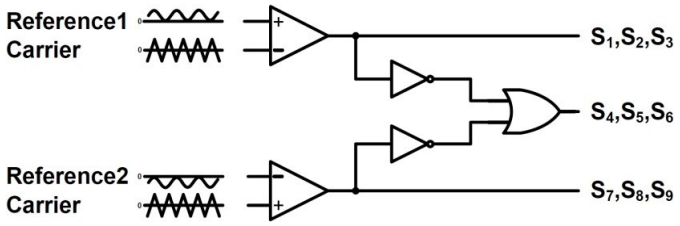

Figure 2-9: The xor signal.

To operate in the linear modulation region of the SPWM, the two reference signals are constrained to stay within the horizontal band of the carrier signal without overlapping, therefore the following inequality has to be satisfied: $m_2 + m_1 \leq 1$ where m_1 and m_2 respectively are the modulation indexes of the two reference signals[18].

2.5.4 NSI switching states

Each of the three legs of the NSI is composed of a three switches and only one switch is allowed to be open, at time, in each leg, to avoid :

- supplying two loads at the same time which will lead to loss of independency of control.
- keeping terminals of any of the two motors open-circuited.

Therefore, a combination of 27 switching states are allowed in the control of NSI. Each leg can be in three different switch ON-OFF position. These positions are referred as (1),(0), and (-1) as it is illustrated in Table2.1. J refers to leg A, B, or C and U, M, L refers to upper, middle and lower semiconductor, respectively[18].

Table 2.1: NSI leg states.

leg state	0	1	-1
SJU	OFF	ON	ON
SJM	ON	OFF	ON
SJL	ON	ON	OFF

Table 2.2 shows that the NSI can supply two motors at the same time if their stator flux space vectors are in the same or neighboring sectors. When the motors are running at the same speed, this holds true for a longer period of time (i.e., which is usually the case, when the EV is going in a straight line).

Table 2.2: Switching vector of NSI.

V_xV_y	$legA$	$legB$	$legc$	type
V_7V_0	1	1	1	
V_7V_7	0	0	0	Zero vector
V_0V_0	-1	-1	-1	
V_1V_0	1	0	0	
V_2V_0	1	1	0	
V_3V_0	0	1	0	
V_4V_0	0	1	1	Upper active vector
V_5V_0	0	0	1	
V_6V_0	1	0	1	
V_7V_1	-1	1	1	
V_7V_2	-1	-1	1	
V_7V_3	1	-1	1	
V_7V_4	1	-1	-1	Lower active vector
V_7V_5	1	1	-1	
V_7V_6	-1	1	-1	
V_1V_1	-1	0	0	
V_2V_2	-1	-1	0	
V_3V_3	0	-1	0	
V_4V_4	0	-1	-1	Same active vector
V_5V_5	0	0	-1	
V_6V_6	-1	0	-1	
V_2V_1	-1	1	0	
V_2V_3	1	-1	0	
V_4V_3	0	-1	1	
V_4V_5	0	1	-1	Middle active vector
V_6V_5	1	0	-1	
V_6V_1	-1	0	1	

All acceptable states of the three legs are shown in Tables 2.1 and 2.2. Due to the aforementioned limitation, only 27 states are permitted, which may be divided into five categories:

- **Zero vectors:** Both outputs are in zero state. In zero state, a load is short-circuited through one of the DC rails.
- **Upper active vectors:** Upper output is in active state but lower output is in zero state.
- **Lower active vectors:** Lower output is in active state but upper output is in zero state.
- **Same active vectors:** Both outputs are in similar active state.
- **Middle active vectors:** Outputs are in different active states (neighbor active states).

These NSI states are also denoted as V_xV_y where V_x refers to the voltage space vector of the upper 'sub-inverter' whereas V_y refers to the voltage space vector of the lower 'sub-inverter', referring to the 27 switching combinations.We can notice that the NSI has two modes of operation. Mode 1, where loads can be supplied simultaneously for only a limited number vectors (Same Active vectors and Middle active vectors). In mode 2, loads of the NSI can be driven in alternate manner either for all possible combinations or only for the remaining switching combinations from mode 1. It should be noted that in the alternate supply by the NSI (i.e., mode 2), when one load is in active state (i.e., supplied by the NSI) the second load is in zero state (i.e., its three terminals are shorted to one of the DC rails.) and vice versa. The sum of modulation indices of the two 'sub-inverters' can reach up to 1.15. On the other hand, when loads of the NSI are supplied simultaneously, the middle switches are all ON (i.e., closed) and therefore the NSI behaves as an ordinary two-level inverter supplying two loads in parallel. In this case, modulation indices of each of the two loads can be reach up to 1.15 .In addition ,if two Y-connected loads are to be driven by the NSI, the peak fundamental phase voltage of each load is given in equation 2.14 [18]:

$$V_{an_{peak}} = Mi * \frac{V_{in}}{2} \tag{2.14}$$

2.6 Simulation and results of PWM-NSI

To test the feasibility of the suggested structure,NSI simulation was run in MATLAB Simulink. In order to achieve the line to line and phase voltages output waveform, a nine-switch inverter with three phase resistive load is shown in Figure 2-10 and Figure 2-12 shows the results.

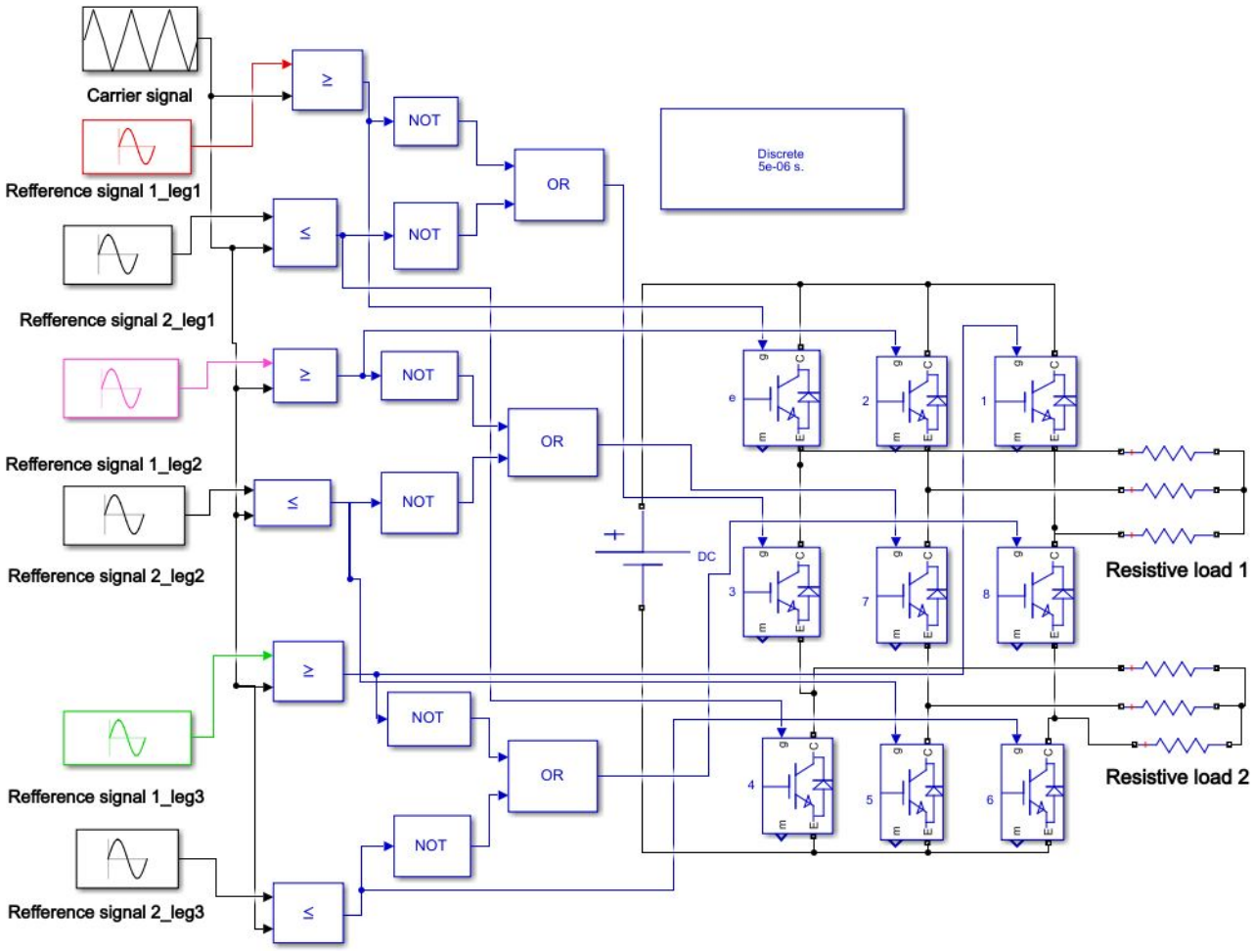

Figure 2-10: A nine-switch inverter with three phase resistive load.

The references sine waves have frequency of 50HZ, 100HZ the upper and lower waves respectively .The output voltage waveforms for both inverters are produced using a 5 KHz carrier frequency and a 400 v dc link .

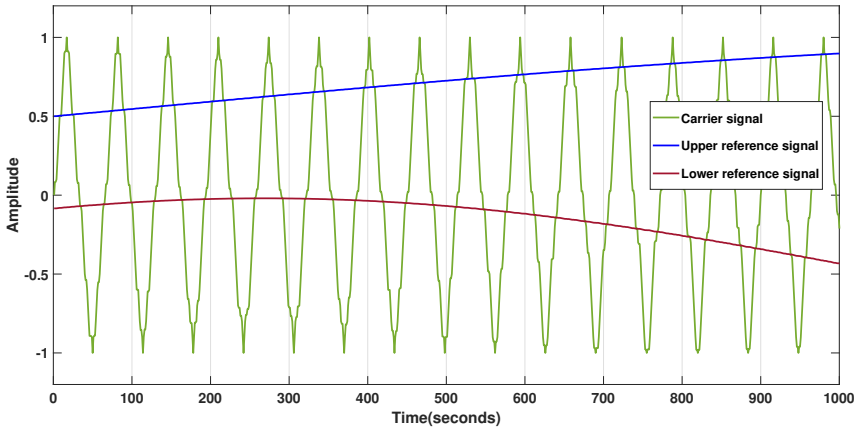

Figure 2-11: Carrier signal with the references.

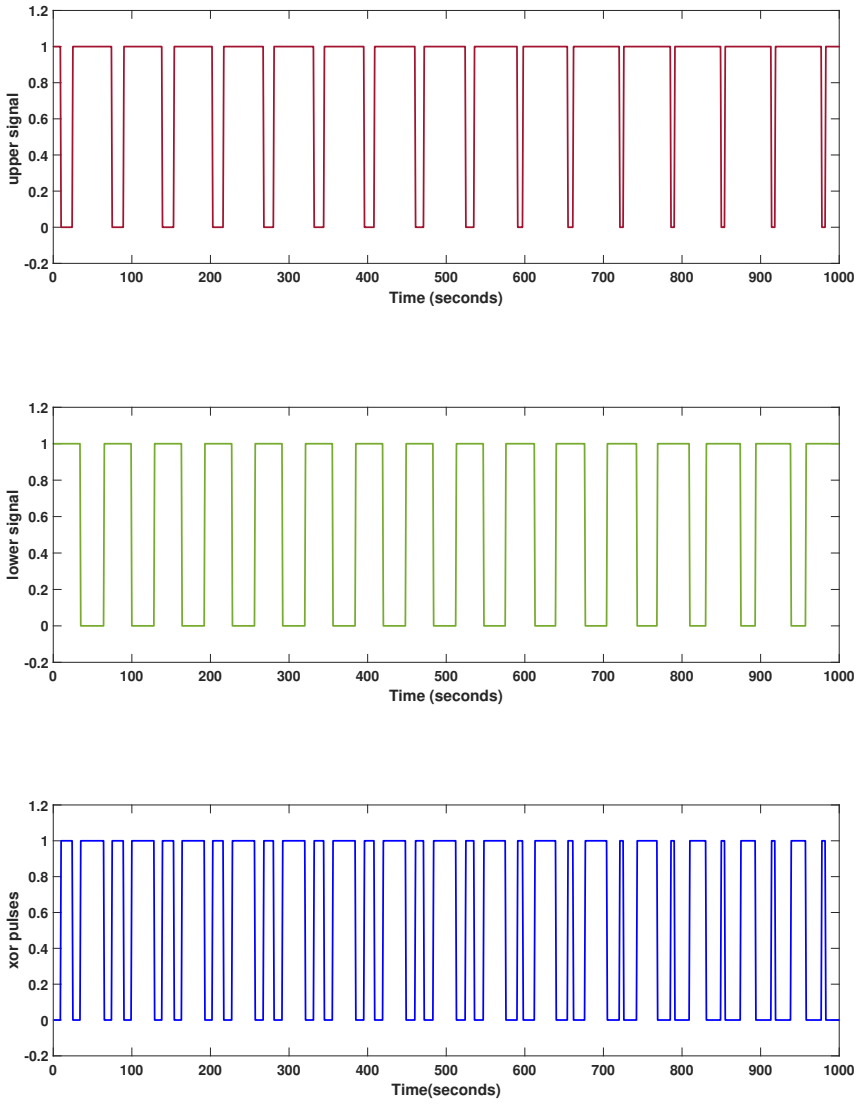

Figure 2-12: The three gate pulses of first leg.

we can notice that the upper and the lower signal never equal to 0 at the same time and the middle pulses are generated by xor of the upper and the lower signals. The line to line and phase voltages are illustrated in Figures 2-13,2-14,2-14 and 2-16,respectively.

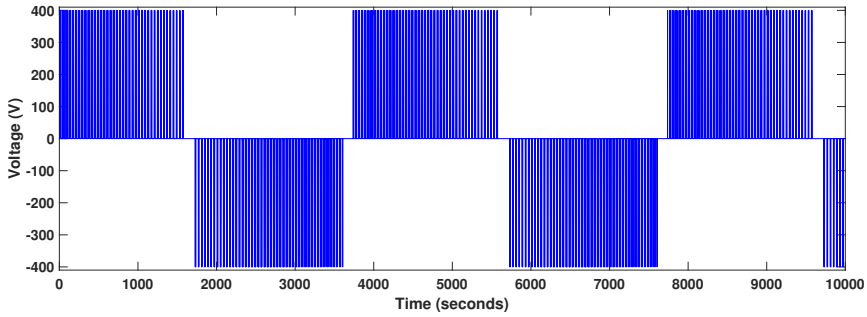

Figure 2-13: Line to line voltage of first load.

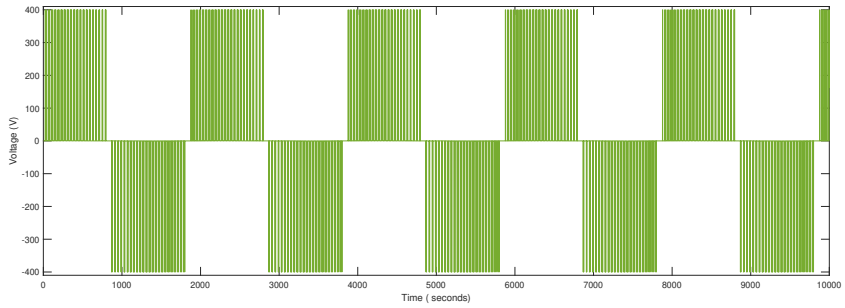

Figure 2-14: Line to line voltage of second load.

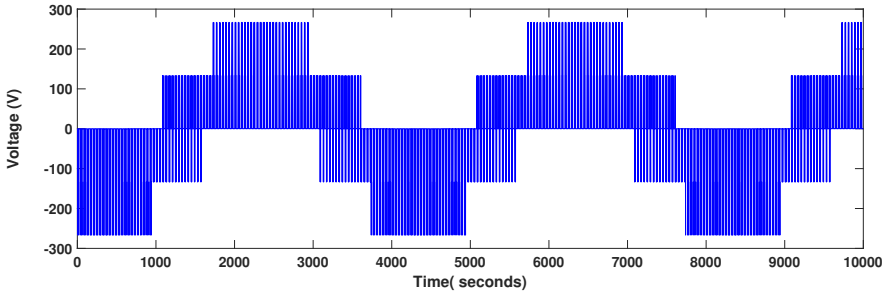

Figure 2-15: Phase voltage of first load.

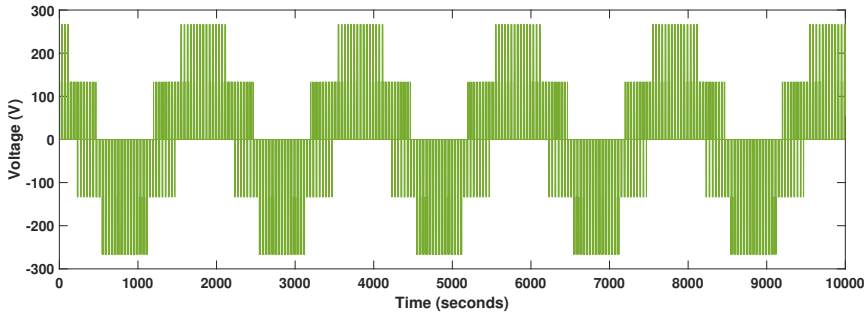

Figure 2-16: Phase voltage of second load

These results indicates that the nine switch inverter can indpendently control amlitude and frequency for two three phase loads.

2.7 Conclusion

We covered the induction motor modeling technique, as well as the six-switch and nine-switch voltage source inverters, in this chapter. A basic introduction to induction motor drives has also been provided, as well as a general classification of control techniques. The following chapter will focus at the essentials of DTC, which is used to drive asynchronous induction motors.

Chapter 3

Direct torque control of induction motor

3.1 Introduction

Theoretical principles of direct torque control (DTC) for high-performance drives were introduced in the second half of the 1980s .Compared with field-oriented control, with origins that date back to the beginning of the 1970s, DTC is a significantly newer concept. While vector control predominantly relies on mathematical modeling of an induction machine, DTC makes direct use of physical interactions that take place within the integrated system of the machine and its supply. The DTC scheme adopts simple signal processing methods and relies entirely on the non ideal nature of the power source that is used to supply an induction machine within the variable speed drive system (two-level or three-level voltage source inverters, matrix converters, etc.). It can therefore be applied to power electronic converter-fed machines only.

3.2 Principle of operation

AC drives based on Direct Torque Control (DTC) of induction machines allow high dynamic performance to be obtained with very simple control schemes. DTC requires set points of flux and torque as independent inputs. The estimated values of these quantities are needed to establish closed loop control of the flux and torque. However, the errors between the estimates of actual quantities and set points are used in a completely different way compared to vector control. There is no utilization of current controllers in DTC. The torque and flux controllers are two-level or three-level hysteresis controllers, which determine whether an increase or a decrease of flux and/or torque is required, depending on whether or not torque or flux errors fall outside the predefined ranges. From this information, together with the knowledge of the

position of the stator flux linkage space vector, an appropriate voltage vector will be selected based on the switching strategy. An accurate knowledge of the magnitude of the stator flux linkage space vector in the machine is needed. However, knowledge of the precise value of the stator flux space vector instantaneous position is not required. The control system only needs to know in which sector of the voltage vector space, which is a two dimensional complex plane, the flux linkage space vector is. In the case of the standard two-level voltage source inverter, there are six sectors in the space vector plane corresponding to the six active voltage space vectors, with the voltage vectors positioned at the centers of the sectors. Each sector expands 60 degrees so that all six of them cover the voltage vector complex plane. The block diagram of the DTC scheme is shown in Figure 3-1[19].

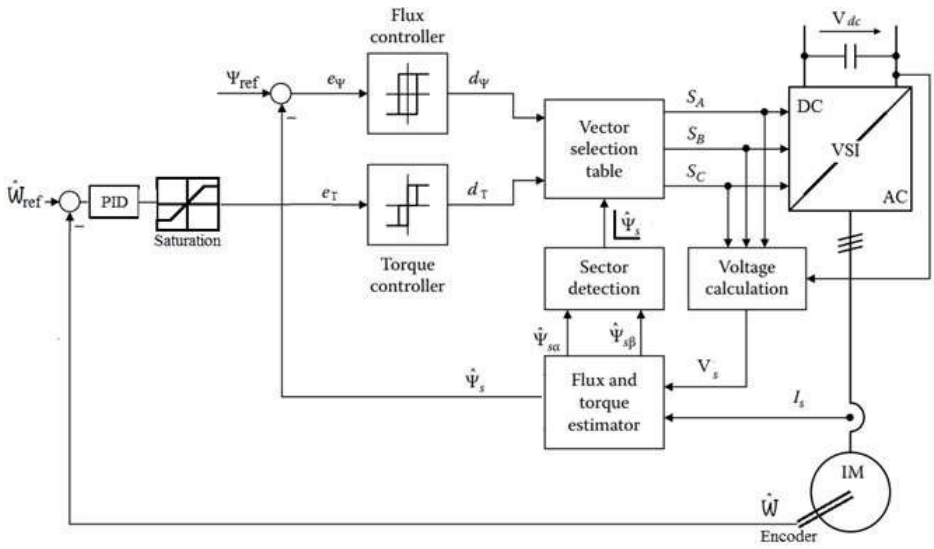

Figure 3-1: Principle of working of DTC.

3.3 Flux controller

The stator flux $\Delta\phi_s$ varies due to the applied stator voltage vector V_s during an interval of time (Δt). As it is shown in equation 3.1:

$$\Delta\phi_s = V_s * \Delta t - R_s * I_s * \Delta t \tag{3.1}$$

We can neglect the stator resistance voltage drop R_s is compared to Vs for high speed regions. Then equation 3.1 can be written as:

$$\Delta\phi_s = V_s * \Delta t \tag{3.2}$$

Therefore, the stator flux is controllable if a proper selection of the voltage vector is made.

(Δt) depends on how long it takes for the torque waveform to move from upper to the lower band as shown by Figure 3-2[20].

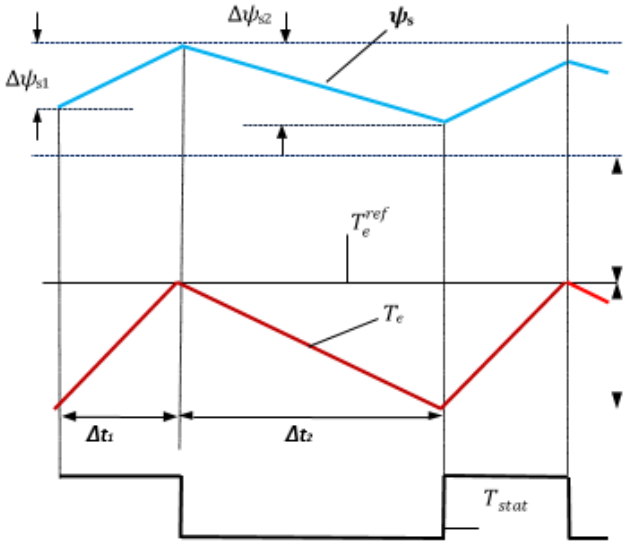

Figure 3-2: Ripples in flux and torque.

The stator flux vector's extremity moves in direction given by the voltage vector and making a circular trajectory as it is illustrated in Figure 3-3.

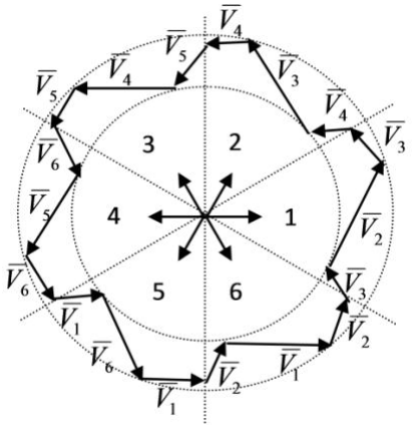

Figure 3-3: Circular trajectory of the stator flux.

A two-level hysteresis comparator is used for flux regulation. It allows to drop easily the flux vector extremity within the limits of the two concentric circles with close radius, as shown in Figure 3-4. The choice of the hysteresis bandwidth h_{ϕ_s} depends on the switching frequency of the inverter.

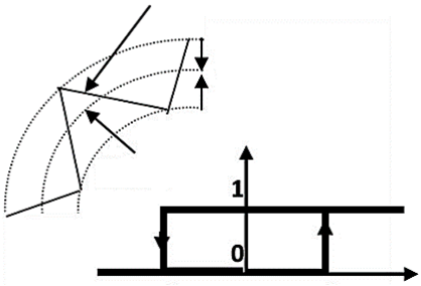

Figure 3-4: Two-level hysteresis comparator for stator flux control.

The logical outputs of the flux controller are defined as:

$$\begin{cases} cflx = 1 \;\; if \;\; \Delta\phi_s > h_{\phi_s} \\ cflx = 0 \;\; if \;\; \Delta\phi_s < -h_{\phi_s} \end{cases} \tag{3.3}$$

$h_{\phi_s}$is hysteresis band of stator flux .The stator flux error is defined by the difference between the references value of flux and the actual estimated value[15]:

$$\Delta\phi_s = |\phi_s^*| - |\phi_s| \tag{3.4}$$

3.4 Control of electromagnetic torque

During one sampling period, the rotor flux vector is supposed invariant. The torque of induction motor can be expressed in terms of stator and rotor flux vectors as follows:

$$T_e = p * \frac{M_{sr}}{\sigma L_s L_r} \vec{\phi_s} \times \vec{\phi_r} \tag{3.5}$$

$$|T_e| = p * \frac{M_{sr}}{\sigma L_s L_r} |\phi_s| \times |\phi_r| \sin(\delta) \tag{3.6}$$

where:

p is the number of poles pairs. ϕ_s, ϕ_r are stator and rotor flux vectors. δ angle between the stator and rotor flux vectors. From expression 3.6 , it is clear that the electromagnetic torque is controlled by the stator and rotor flux amplitudes. If those quantities are maintaining constant, the torque can be controlled by adjusting the load angle δ. The torque regulation can be realized using three-level hysteresis comparator (see Figure3-5). It allows to control the motor in both rotation senses. The two-level comparator can be used for one rotation sense.

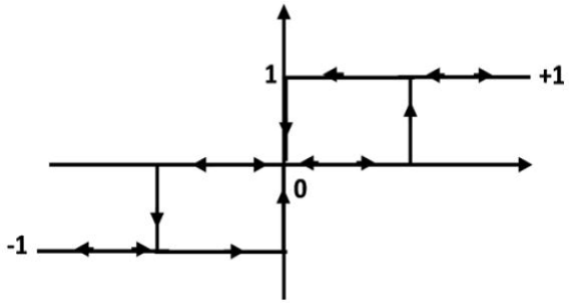

Figure 3-5: Three level hysteresis comparator for electromagnetic torque control.

The logical outputs of the torque controller are defined as:

$$\begin{cases} ctrq = 1 \;\; if \;\; \Delta T_e > h_{T_e} \\ ctrq = 0 \;\; if \;\; -h_{T_e} < \Delta T_e < h_{T_e} \\ ctrq = -1 \;\; if \;\; \Delta T_e < -h_{T_e} \end{cases} \tag{3.7}$$

Where h_{T_e} is hysteresis band of torque. The torque error is defined by the difference between the references values of the torque and the actual estimated values[15]:

$$\Delta T_e = T_e^* - T_e \tag{3.8}$$

The amplitude of the hysteresis band greatly influences the drive performance such as flux and torque ripples, inverter switching frequency, and current harmonics. Therefore, the magnitude of the hysteresis band should be determined based on reasonable guidelines which can avoid excessive inverter switching frequency and current harmonics in the whole operating region[21].

3.5 Estimation of stator flux and electromagnetic torque

DTC asks for the estimation of stator flux and the motor torque, so that closed loop flux and torque control can be established[15].

3.5.1 Stator flux estimation

The estimation of the stator flux is usually done by the integration of the back EMF. The stator flux components can be expressed using stator voltages and currents in the stationary

reference frame (α, β) by:

$$\phi_{s\alpha} = \int (V_{s\alpha} - R_s * I_{s\alpha})dt \tag{3.9}$$

$$\phi_{s\beta} = \int (V_{s\beta} - R_s * I_{s\beta})dt \tag{3.10}$$

The stator flux magnitude and flux angle can be computed as:

$$\phi_s = \sqrt{\phi_{s\alpha}^2 + \phi_{s\beta}^2} \tag{3.11}$$

$$\theta_s = \tan^{-1}(\frac{\phi_{s\beta}}{\phi_{s\alpha}}) \tag{3.12}$$

The stator voltage components $V_{s\alpha}$,$V_{s\beta}$ are obtained by applying Concordia transformation on the output voltage of the three-phase VSI:

$$\begin{bmatrix} V_{s\alpha} \\ \\ V_{s\beta} \end{bmatrix} = \begin{bmatrix} 1 & \frac{-1}{2} & \frac{-1}{2} \\ \\ 0 & \frac{\sqrt{3}}{2} & \frac{-\sqrt{3}}{2} \end{bmatrix} \begin{bmatrix} V_{sa} \\ V_{sb} \\ V_{sc} \end{bmatrix} \tag{3.13}$$

The stator currents components $I_{s\alpha}, I_{s\beta}$ can be obtained also by applying Concordia transformation on the measured currents:

$$I_{s\alpha} = \sqrt{\frac{2}{3}} I_{sa} \tag{3.14}$$

$$I_{s\beta} = \frac{1}{\sqrt{2}}(I_{sb} - I_{sc}) \tag{3.15}$$

3.5.2 Electromagnetic torque estimation

The produced electromagnetic torque of the induction motor can be determined using the cross product of the stator quantities (i.e., stator flux and stator currents). The torque formula is expressed as following:

$$T_e = p(\phi_{s\alpha} I_{s\beta} - \phi_{s\beta} I_{s\alpha}) \tag{3.16}$$

3.6 Switching table

From the considerations of the previous section, it follows that for successful operation of a DTC scheme, it is necessary to have accurate estimates of the stator flux amplitude and the electromagnetic torque. In addition,it is necessary to estimate in which sector of the complex plane the stator flux space vector is situated.Considering the six sectors shown in Figure 2-6,the

stator flux switching sectors can be distributed as follows:

$$\begin{cases} \frac{-\pi}{6} < \theta_{s1} < \frac{\pi}{6} \quad ; \quad \frac{\pi}{6} < \theta_{s2} < \frac{\pi}{2} \\ \frac{\pi}{2} < \theta_{s3} < \frac{5\pi}{6} \quad ; \quad \frac{5\pi}{6} < \theta_{s4} < \frac{7\pi}{6} \\ \frac{7\pi}{6} < \theta_{s5} < \frac{3\pi}{2} \quad ; \quad \frac{3\pi}{2} < \theta_{s6} < \frac{11\pi}{6} \end{cases}$$

Equation 3.12 can be used to find the location of the stator flux space vector in the complex plane.

While the stator flux vector is located in the sector i we have :

- If V_{i+1} is selected,ϕ_s increases and T_e increases.
- If V_{i-1} is selected,ϕ_s increases and T_e decreases.
- If V_{i+2} is selected,ϕ_s decreases and T_e increases.
- If V_{i-2} is selected,ϕ_s decreases and T_e decreases.

For each sector, the vectors V_i and V_{i+3} are not considered because both of them can increase or decreases the torque in the same sector according to the position of flux vector on the first or the second sector. If the zero vectors V_0 and V_7 are selected, the stator flux will stop moving and its magnitude will not change, the electromagnetic torque will decrease, but not as much as when the active voltage vectors are selected. The resulting look-up table for DTC which was proposed by Takahashi is presented in Table 3.1[15].

Table 3.1 gives the optimum selection of the voltage vectors for all the possible stator flux space vector positions (in terms of sectors) and the desired control inputs, which are the output of the torque and flux hysteresis comparator, respectively. The outputs will give commands of increase or decrease for torque and stator flux, in order to keep both of them within the respective hysteresis band. If a stator flux increase is required, then $\Delta\phi_s = 1$, and if a stator flux decrease is required, then $\Delta\phi_s = 0$. Similarly, if a torque increase is required, then $\Delta T_e = 1$, if a torque decrease is required, then $\Delta T_e = -1$ and if no change in torque is required, then $\Delta T_e = 0$.

Table 3.1: The switching vectors in the different stator flux sectors.

$Flux$	$Torque$	$Sector1$	$Sector2$	$Sector3$	$Sector4$	$Sector5$	$Sector6$
$cflx = 1$	$ctrq = 1$	v_2	v_3	v_4	v_5	v_6	v_1
	$ctrq = 0$	v_7	v_0	v_7	v_0	v_7	v_0
	$ctrq = -1$	v_6	v_1	v_2	v_3	v_4	v_5
$cflx = 0$	$ctrq = 1$	v_3	v_4	v_5	v_6	v_1	v_2
	$ctrq = 0$	v_2	v_3	v_4	v_5	v_6	v_1
	$ctrq = -1$	v_2	v_3	v_4	v_5	v_6	v_1

3.7 Speed control

A PID controller is used as a speed controller whose input is the error between the speed command and feedback speed. Feedback speed can be from the speed sensor or speed estimator. A PI controller is commonly used instead of a PID controller. For better performance of speed responses (lower overshoot, faster time response, reduced or zero steady-state error), a PI controller with anti-wind up is used as a speed controller. The poles placement method is used to determine the controller gains. The used PI controller in our work in the outer speed loop is the anti-windup controller. It allows to enhance speed control performance by cancelling the windup phenomenon which is caused by the saturation of the pure integrator. This strategy consists on the correction of the integral action based on the difference between the control signal and the saturation limit. The difference value is passed through a gain block (tracking time constant T_i) before arriving as feedback to the integrator[3].

3.8 Simulation results

To study the performance of the developed DTC model, a closed loop speed control of a $1.1Kw$ induction motor (with characteristics given in the appendix) is simulated using MATLAB/Simulink simulation package. Figure 3-6 presents the developed simulation model.

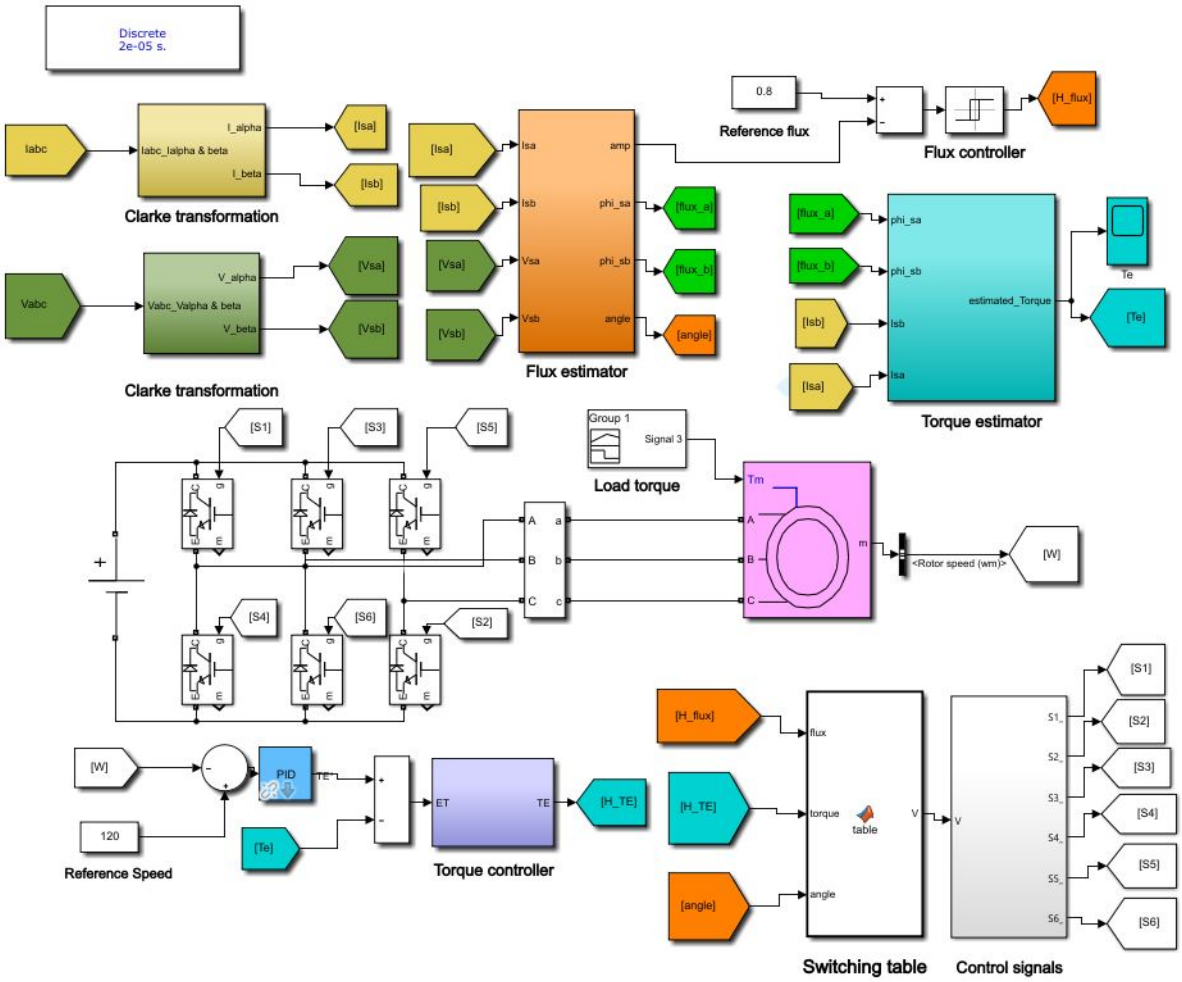

Figure 3-6: Simulink block diagram of the developed DTC.

The simulation was carried out under the following conditions:

- The torque comparator hysteresis band is ± 0.05 Nm.
- The flux comparator hysteresis band is ± 0.005Wb.
- The reference electromagnetic torque is recovered at the output of the PI controller.
- The reference flux is 0.8 Wb.
- The power sim induction motor model was used.
- A maximum step size of (0.01 ms).

3.8.1 Test 1: No-load start followed by load disturbances

This test will assess the dynamic performance of the proposed DTC model, which will be performed while keeping a speed reference of $(\omega = 120 Rad/s)$. The obtained results of the rotational speed, the electromagnetic torque, the stator currents, the stator flux and the stator

flux trajectory respectively are shown in Figures 3-7,3-8, 3-10, 3-9,3-11.The simulation covered both the starting up and the steady states operation of the controlled motor without/with load.

The test starts with no loaded IM. It can be seen that the rotor speed follows its reference value with no steady state error nor overshoot and a rise time of $(0.17s)$. The starting torque attains a value of $(17Nm)$ and decreases sharply till $(0Nm)$. It is worth noting that both torque and rotor speed reach their expected values at the same time.

At $(t = 0.8s)$,load disturbance of $(5Nm)$ has been introduced. Initially, the speed decreases but The speed regulation loop instantly rejects the supplied load disturbance and reestablishes stability, while the electromagnetic torque rapidly increases to achieve its load reference value of $(5Nm)$ with a slight overshoot $(1Nm)$ owing to the hysteresis controllers used.

The motor is suddenly unloaded at $(t = 1.2s)$, and the rotor speed increases, then recovers and returns to its initial value, while the electromagnetic torque decreases just before returning to near zero.This explain that the DTC attained high dynamic performance in speed response to variations in torque load demand.

It is noticed from Figure 3-9 that the currents magnitude changes with the change in the load torque. Thus, when a load was introduced at $(t = 0.8s)$, the currents magnitude increases in order to satisfies the system requirements and when the motor becomes unloaded,the current goes back to its initial value. It can be observed that the stator current waveforms are sinusoidal in shape.

The stator flux magnitude response has risen to its reference value of $(1Wb)$ and was constrained within its hysteresis band of $(0.005Wb)$ therefore; the flux trajectory draws the figure of a circle of radius (1).Stator flux is not affected during the application and removal of load torque, as shown in Figure 3-10, which causes the variation of the motor's electromagnetic torque. This illustrates the ability of DTC to independently control the torque and flux in the induction motor.

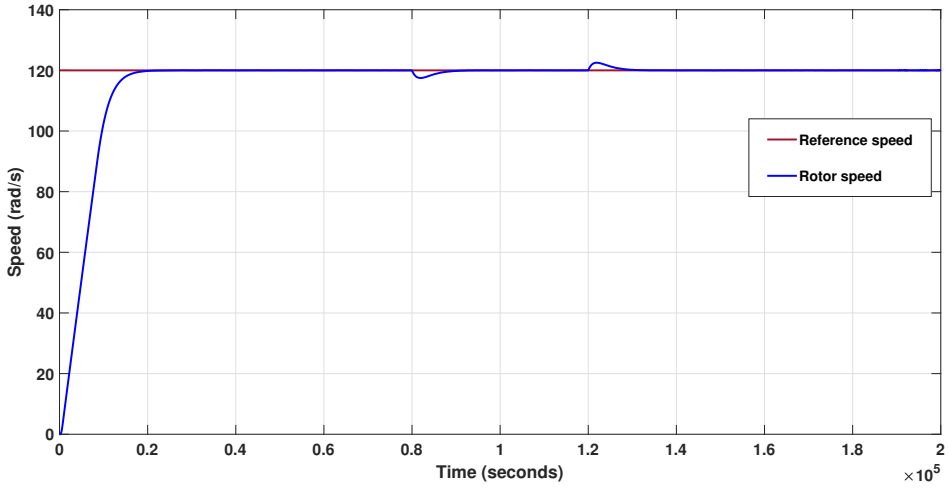

Figure 3-7: Rotor speed.

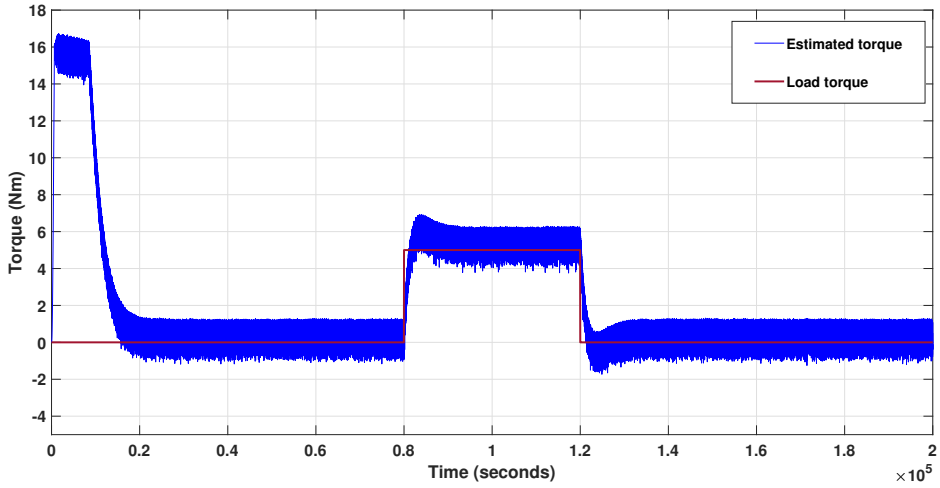

Figure 3-8: Electromagnetic torque.

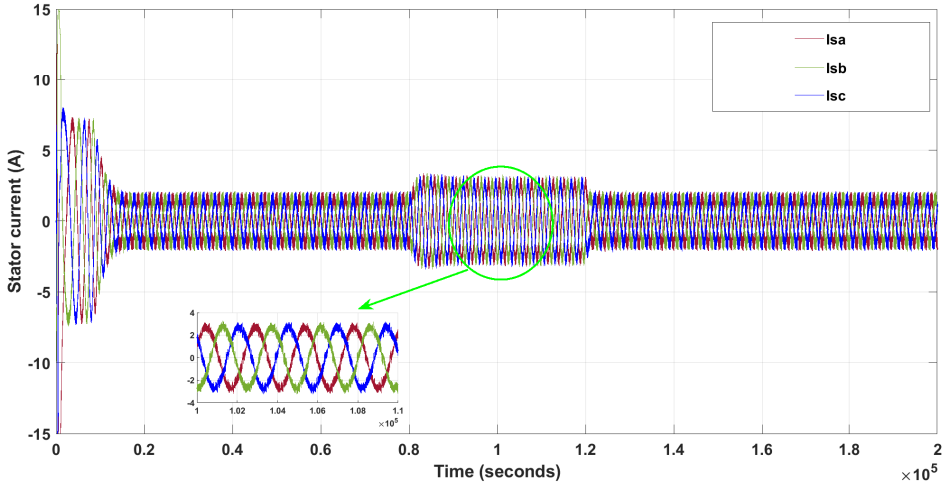

Figure 3-9: Stator current.

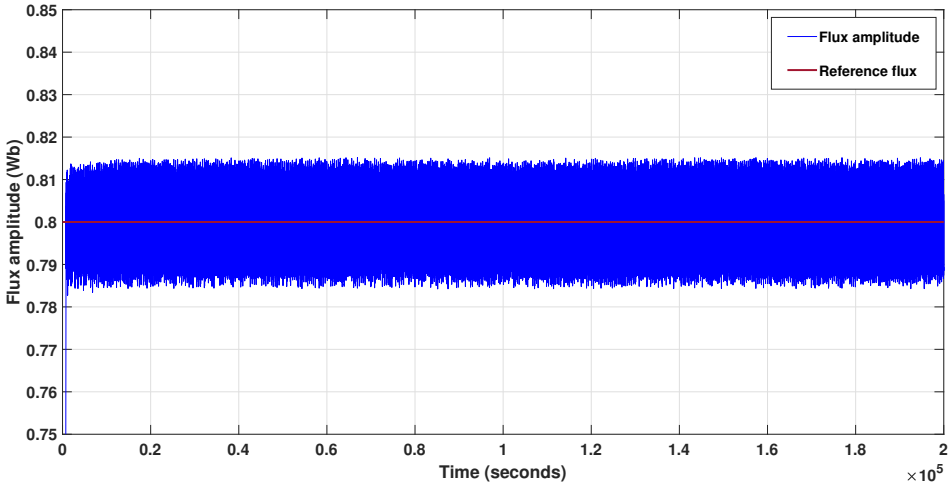

Figure 3-10: Stator flux.

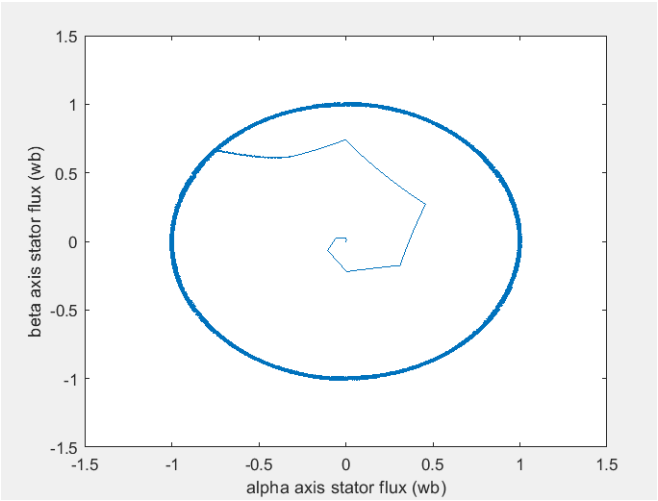

Figure 3-11: Stator flux trajectory.

3.8.2 Test2: Reversed rotation:

The only difference between this test and the previous one was that at $(t = 0.9s)$, the reference speed was changed from $(80Rad/s)$to$(-40Rad/s)$, which was held constant for the rest of the test time. This negative reference value caused the reversal of the rotation.

Figures 3-12,3-13 , 3-14,3-15, 3-16 show the responses of the machine before and during the reversal of the direction of rotation .The simulation results show that there is a good follow-up to the newly applied reference speed of $(-40Rad/s)$ with no overshoot nor steady state error with good both torque and flux responses. Figure 3-14 shows clearly the reverse direction in the three phase current sequence when a negative speed was provided.

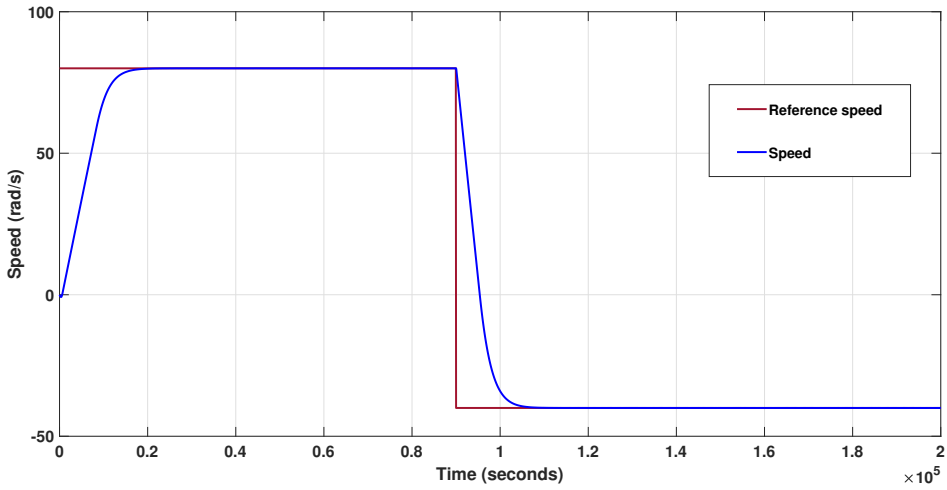

Figure 3-12: Rotor speed.

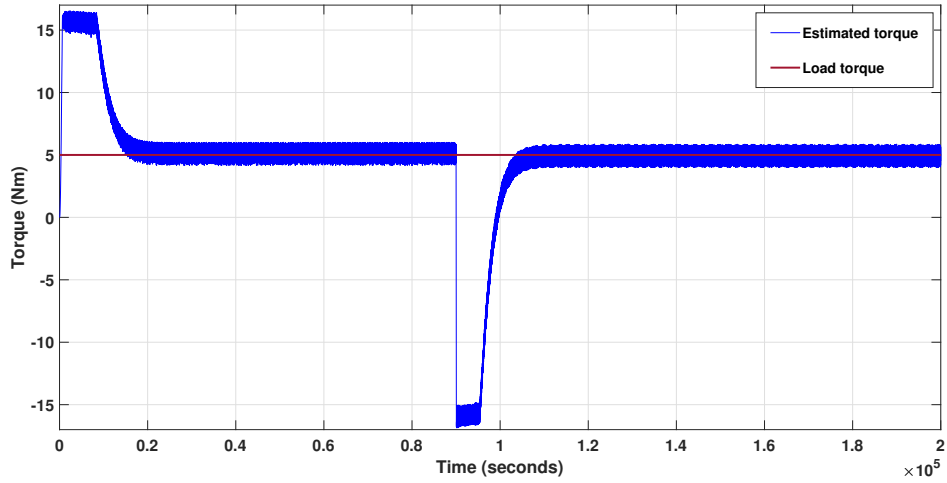

Figure 3-13: Electromagnetic torque.

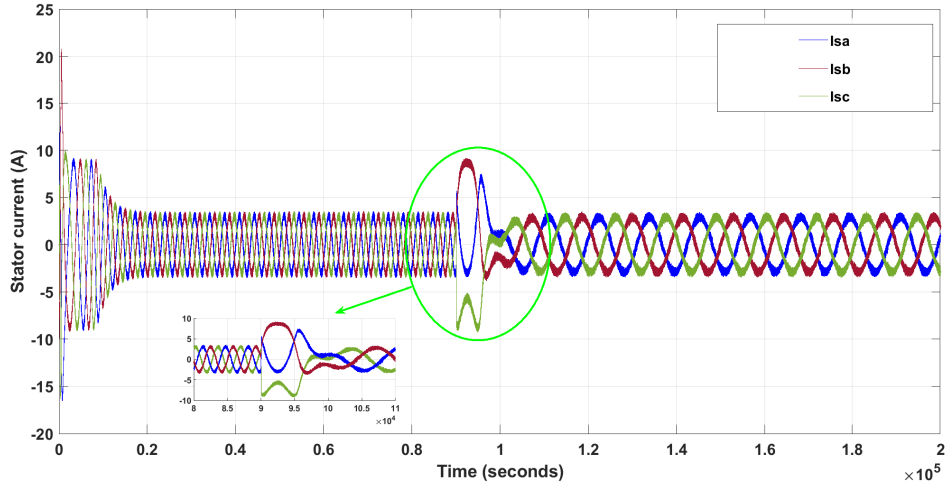

Figure 3-14: Stator current

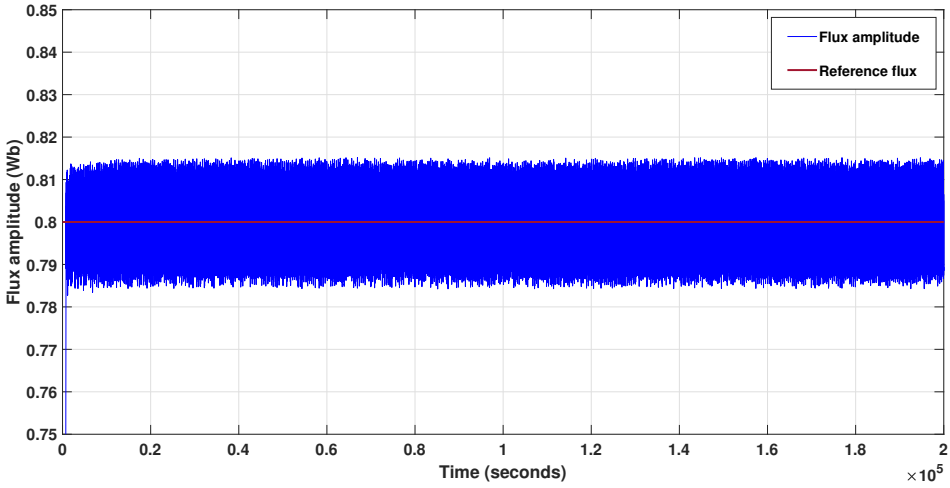

Figure 3-15: Stator flux.

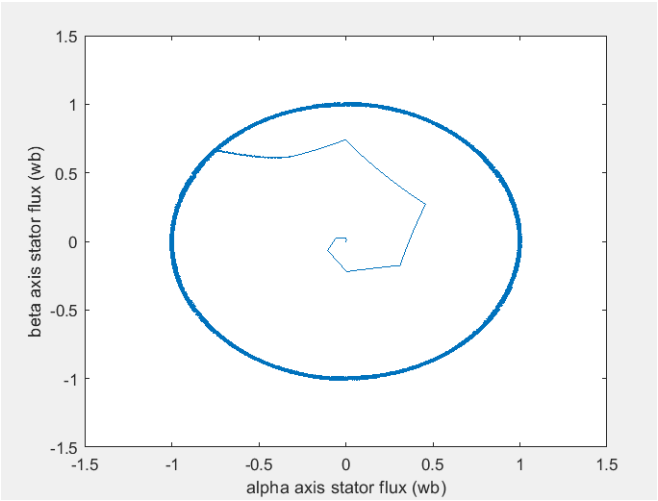

Figure 3-16: Stator flux trajectory

3.9 Conclusion

The operation principles of the direct torque control technique were outlined in this chapter, and a schematic outlining its function was shown. The DTC method appears to be an efficient and simple way of controlling an induction machine. Numerical simulations were successfully done to test the performance of the control approach, followed by discussion and notes of the obtained results, which ultimately confirmed the DTC method's good performance. The DTC technique of two IMs using NSI fed by battery will be discussed in the next chapter.

Chapter 4

Control of electric vehicle traction chain

4.1 Introduction

The prospects of The potential for NSI exploitation in EV applications is massive. The creation of two Direct Torque Control (DTC) schemes to operate two induction motors via the NSI is evidence in favor of this claim.

Regenerative braking is one of the important systems in electric vehicle since it has the ability to save the wastes energy up to 8-25%. This amount of saved energy can be use to extend our daily journey or to be used to power up the accessories in the car. Furthermore, the regenerative braking system has been improved by the advanced power electronic component such as DC-DC Buck Boost converter.

4.2 DTC-NSI driven two IMs

4.2.1 Simulation model and results

In order to demonstrate the independent control of both motors, two identical IMs (with characteristics given in the appendix) are driven with different combinations of speed and torque profiles. Simulation using the Matlab/Simulink software is shown in Figure 4-2 and Figure 4-1.

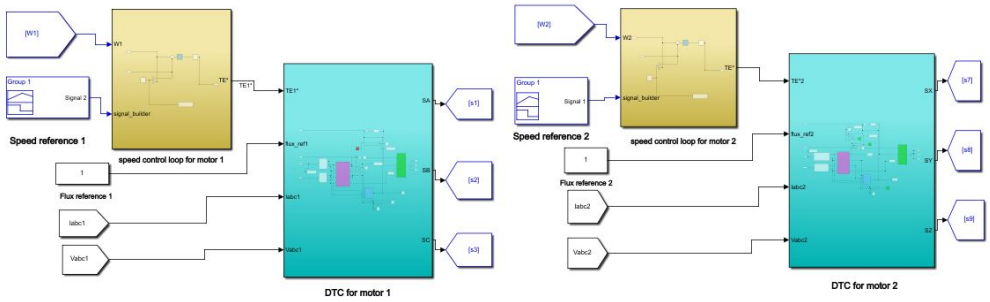

Figure 4-1: DTC-NSI control.

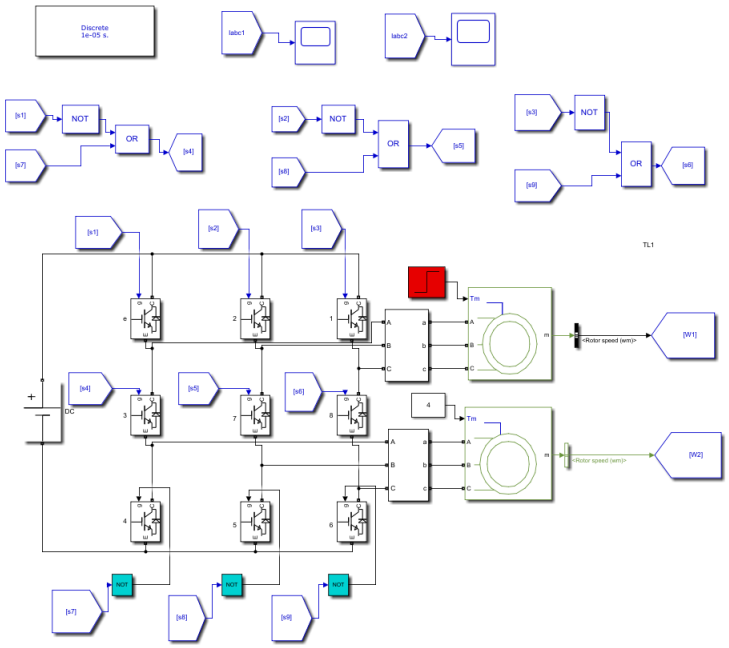

Figure 4-2: NSI drive two three phase motor.

4.2.2 Discussion

First, the speed of the two motors is set to $(\omega = 100Rad/s)$ and $(\omega = 150Rad/s)$,respectively. the system shows a good speed responses for both machines with good tracking and short transient stage with some fluctuations. Due to this high acceleration rate, high starting torque for both motors can be seen. It is requested by the control system to reach the assigned speed in short time.

For the first motor, at $(t = 0.4s)$, a load is coupled and remains for the rest of the test. The estimated torque is inrceased to keep the motor running at the assigned speed, a slight decrease is noticed in the speed due to the load applied.

The reference speed is changed to $(\omega = 120Rad/s)$ at $(t = 0.6s)$ and it is reduced to $(\omega = 90Rad/s)$ at$(t = 1.4s)$ and remains constant until the test is completed. The system response tracks the reference speed accurately. The electromagnetic torque was affected by the

decreasing in the speed at ($t = 1.4s$) ,then, quickly, it recovers its last value.

For the second motor, the load is fixed at ($4Nm$) during all the test. The motor exhibits normal torque response for the DTC method, with a good follow up to the reference torque with in-range torque ripples.

At ($t = 0.9s$), the speed has been reversed to ($\omega = -50Rad/s$). As a consequence, the torque reaches a high negative value equals to the its starting value since the reverse rotation can be considred as a new starting for the motor in opposite direction then it tracks its reference.

Concerning the stator current, for both motor, it takes sinsoidal shape with an envlope aquired from the direct proportional relationship between the current and the torque.

The flux for both motors follows their reference value ($1Wb$) with ripples within the band of the hysteresis controller. We can notice that the flux is not affected by the changing in the torque or speed due to the decoupling achieved by DTC.

Relevant to fluctuations, they can be seen in all Figures, a solution to remove them will be proposed in the next section with details. The corresponding simulation results are illustrated in the next Figures.

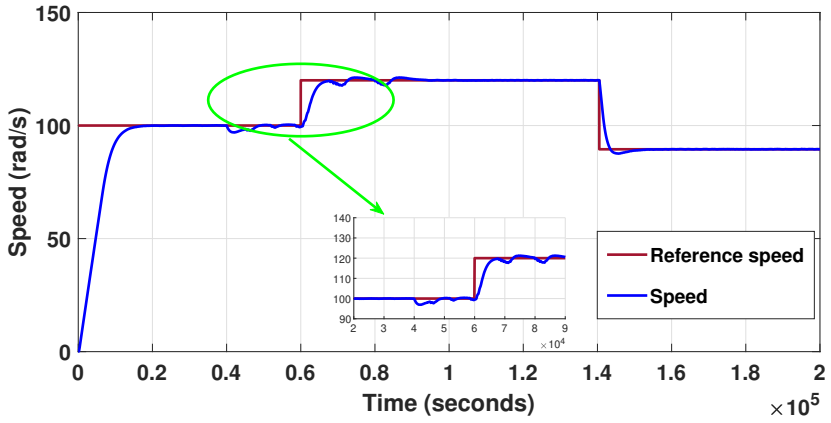

Figure 4-3: Rotor speed for the first motor.

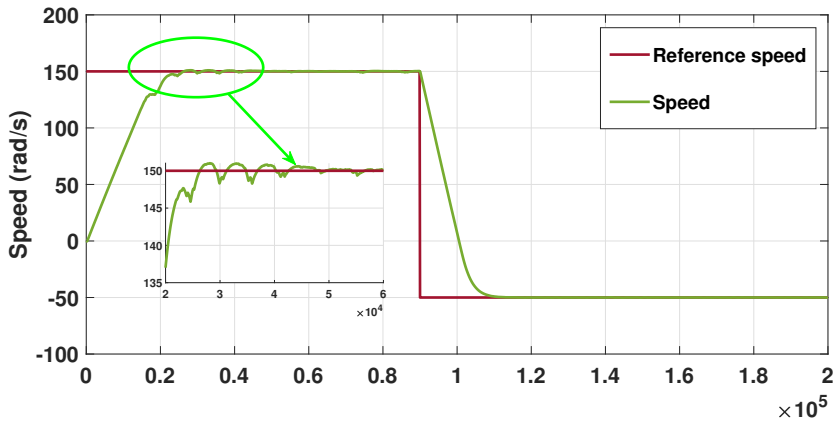

Figure 4-4: Rotor speed for the second motor.

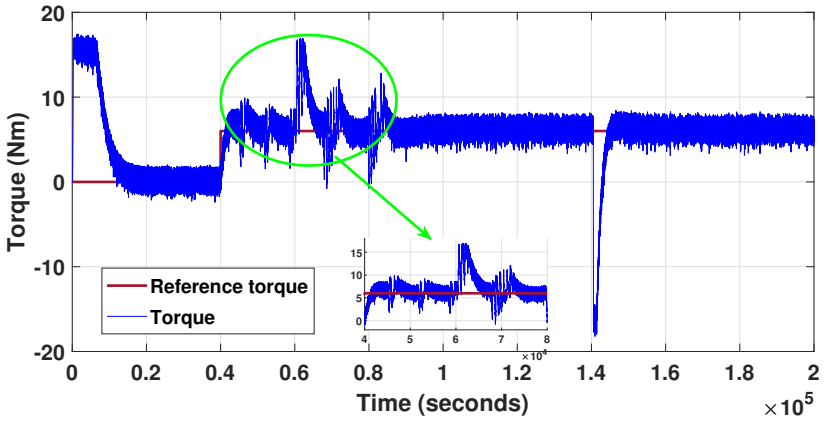

Figure 4-5: Electromagnetic torque for the first motor.

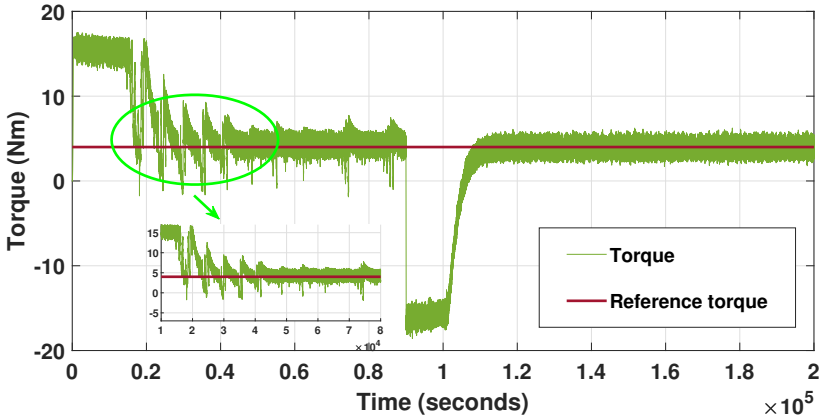

Figure 4-6: Electromagnetic torque for the second motor.

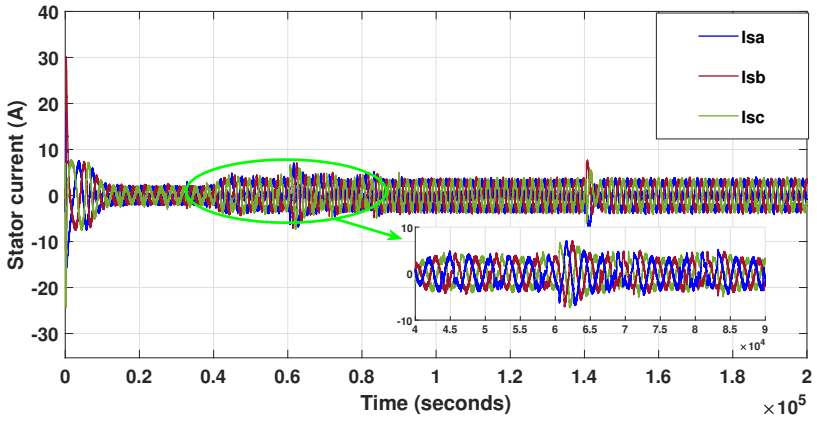

Figure 4-7: Stator current for the first motor.

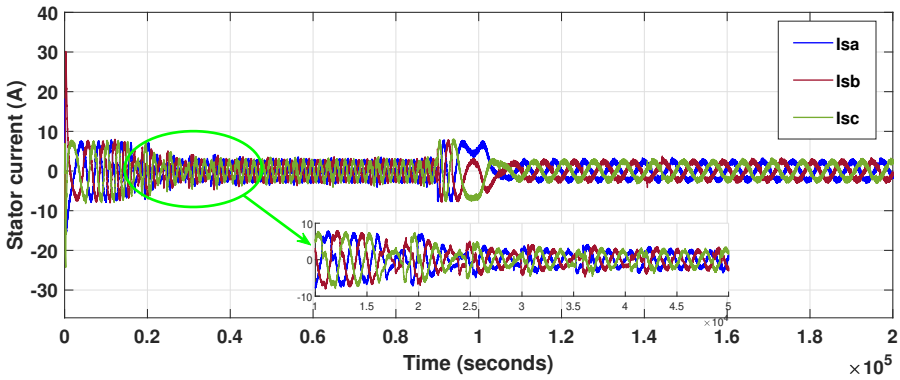

Figure 4-8: Stator current for the second motor.

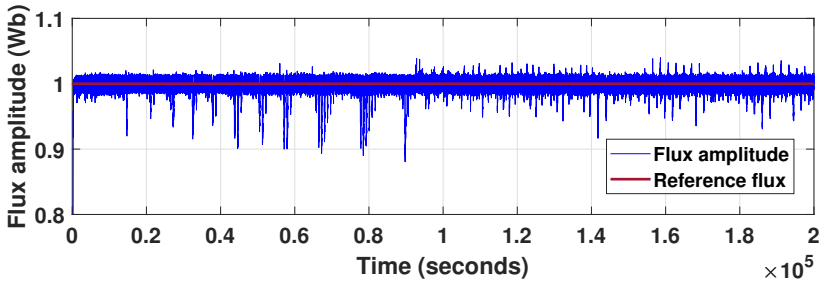

Figure 4-9: Stator flux amplitude for the first motor.

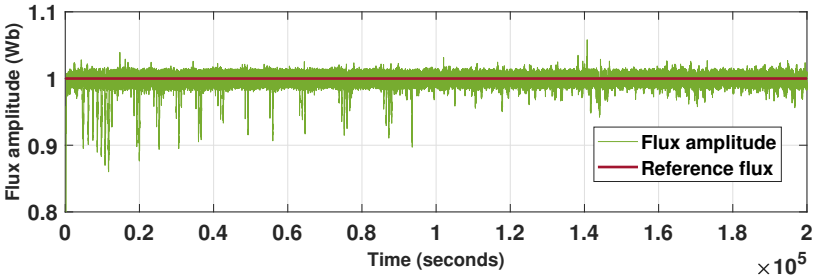

Figure 4-10: Stator flux amplitude for the second motor.

4.3 Synchronization

In DTC control, the application of zero vector has little or no effect on motor's stator flux but the rate of decrease of a motor's torque is directly proportional to the motor's speed of operation leading to large torque ripples, especially if the motor in question is operating in high speed, eventually leading to misoperation of the entire system. To mitigate the effect of significant dip in torque of any of the two motors and to avoid using a faster processing controller, which may erode the simplicity of the DTC control method. The presented algorithm will consider the inputs from the switching tables to ensure the simultaneous supply of the two motors. In the

simultaneous drive of the two motors, faster response is obtained and the modulation indices can be increased to up to 1.15 each, which translate to high torque/speed capabilities. On the other hand, the conceived algorithm is simpler as it does not require reading torque and speed values at each iteration. According to Table 2.2 and based on Figure4-12, the NSI can supply the two motors simultaneously, if the stator flux space vectors of these motors are in the same or neighbouring sectors. This holds true for a longer time, when motors are running at the same speed (i.e., which is usually the case, when the EV is going in a straight line). The flowchart of the suggested algorithm is demonstrated in Figure 4-11.

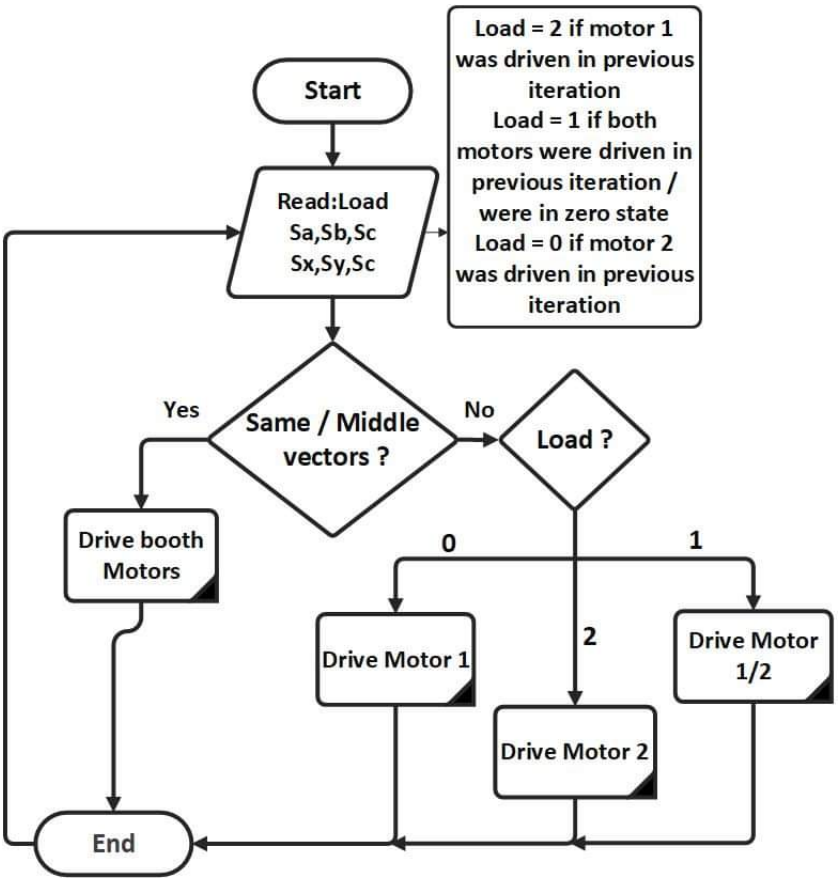

Figure 4-11: Flowchart of the synchronization algorithm [3].

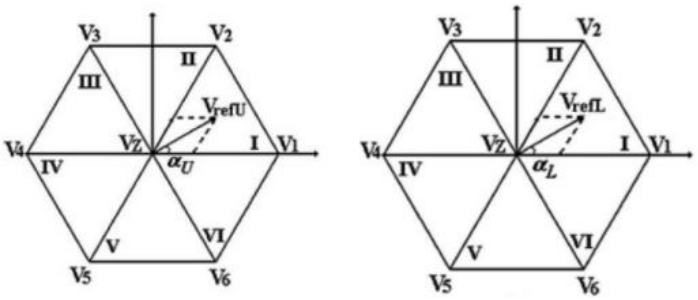

Figure 4-12: Voltage space vector locations [3].

4.3.1 Simulation model and results

A simulation is performed using the MATLAB/Simulink software to show the presented algorithm's viability. Figure4-13 presents the developed simulation model.

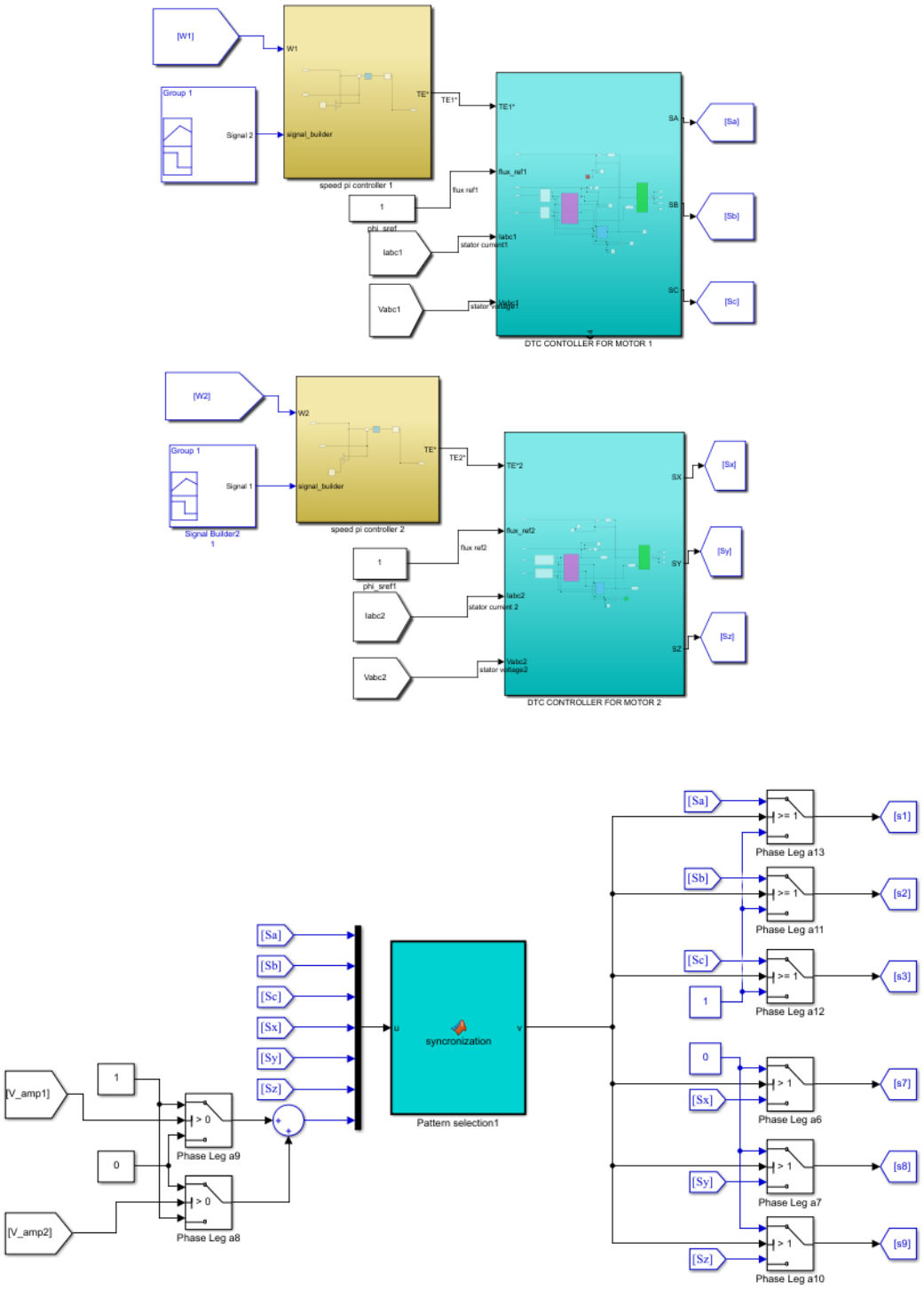

Figure 4-13: Simulation model of DTC-NSI with Synchronization block.

4.3.2 Discussion

From simulation results shown below, for the rotor speed, it can be noticed that the fluctuations in steady state are almost damped and the speed accurately tracks its reference . Additionally,the stator flux amplitude,stator current and the torque response for both motors indicate lower ripples. Hence, the overall performance of the NSI with the synchronization block was clearly improved.

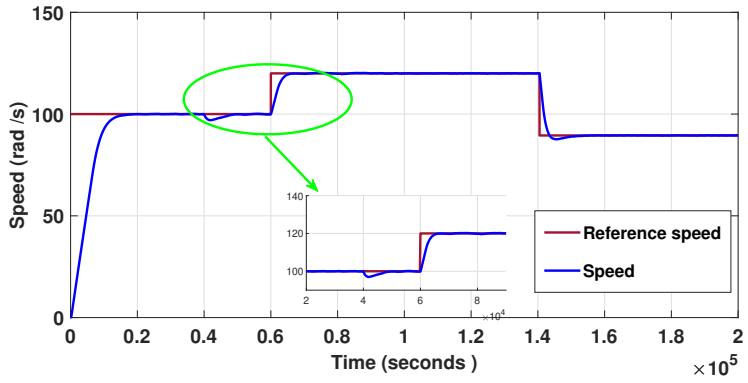

Figure 4-14: Rotor speed for the first motor.

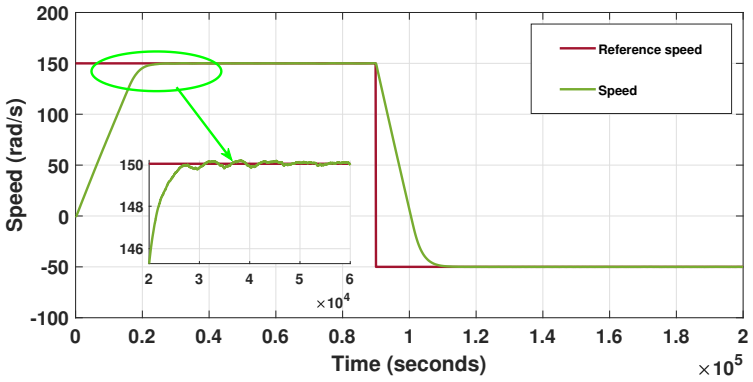

Figure 4-15: Rotor speed for the second motor.

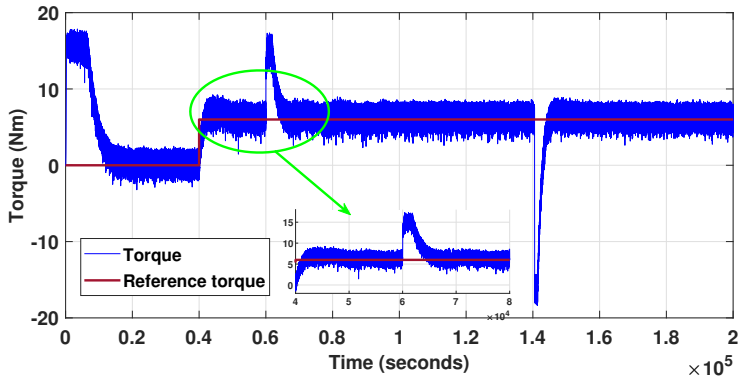

Figure 4-16: Electromagnetic torque for the first motor.

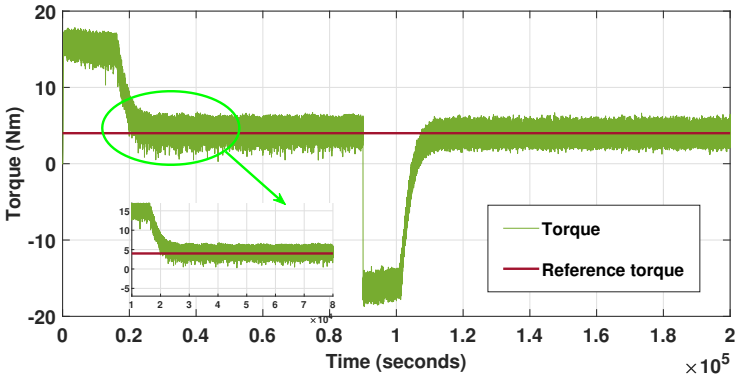

Figure 4-17: Electromagnetic torque for the second motor.

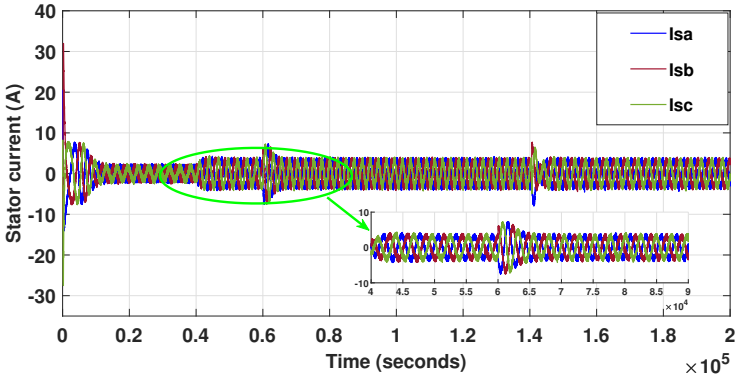

Figure 4-18: Stator current for the first motor.

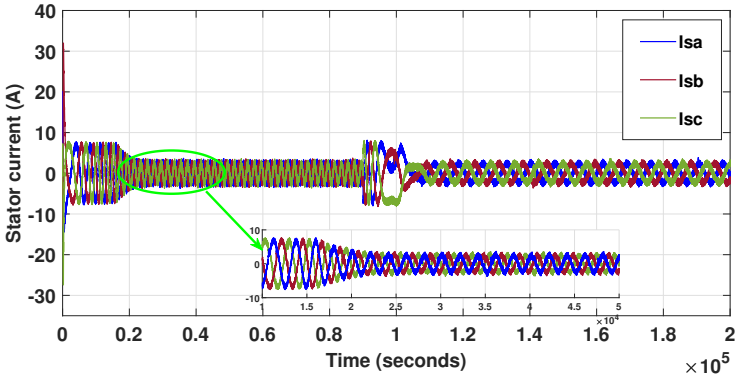

Figure 4-19: Stator current for the second motor.

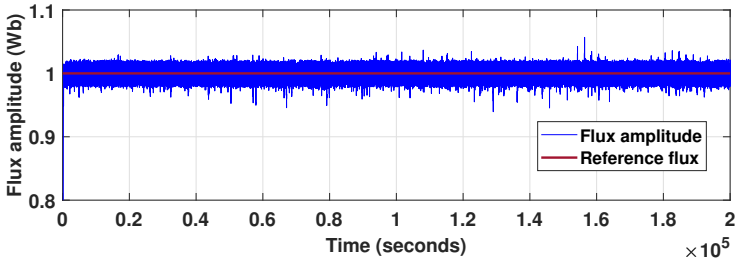

Figure 4-20: Stator flux amplitude for the first motor.

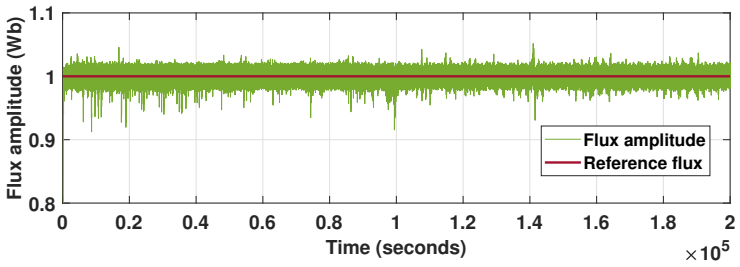

Figure 4-21: Stator flux amplitude for the second motor.

4.4 DTC-NSI fed by DC-DC converter-battery

Energy storage systems, usually batteries, are essential for all electric vehicles. The battery pack consists of large numbers of battery cells arranged in series and parallel to produce the voltage required to power the EV. Most of the time a DC-DC converters are employed to boost the battery terminal voltage to the inverter's input voltage level to supply the load.

A simulation was run using MATLAB/Simulink software to evaluate the DTC with NSI fed by a lithium battery, where various DC-DC converter topologies have been investigated.

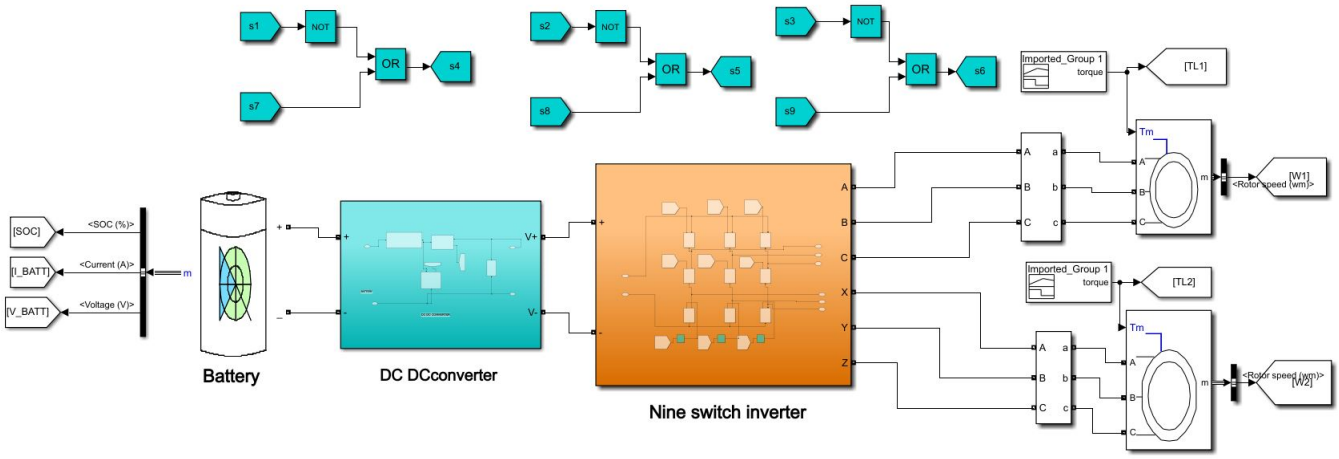

Figure 4-22: General scheme of DTC with NSI fed by Battery.

4.4.1 Inverting buck boost

The Inverting buck boost takes a positive input voltage and converts it to a negative high/low output voltage, with a common ground connection between input and output.

Simulation results and Discussion

To verify the validity of the proposed scheme in boost mode, a simulation model was built

based on Matlab/Simulink with a battery parameters of: rated voltage is 450V, rated capacity of 200 Ah, and the SOC is 100%. The simulation results are shown below.

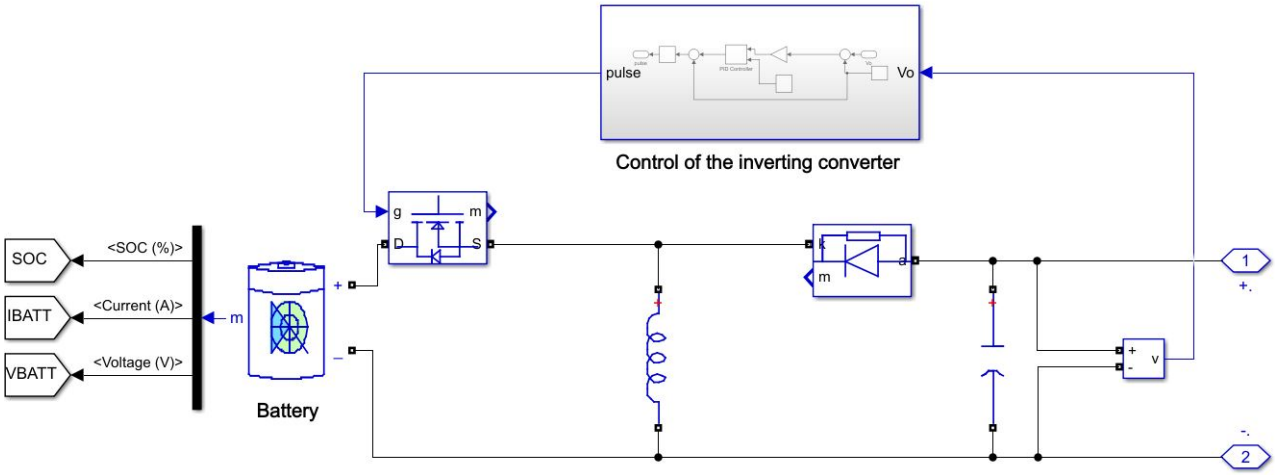

Figure 4-23: Simulink model of Inverting buck boost converter.

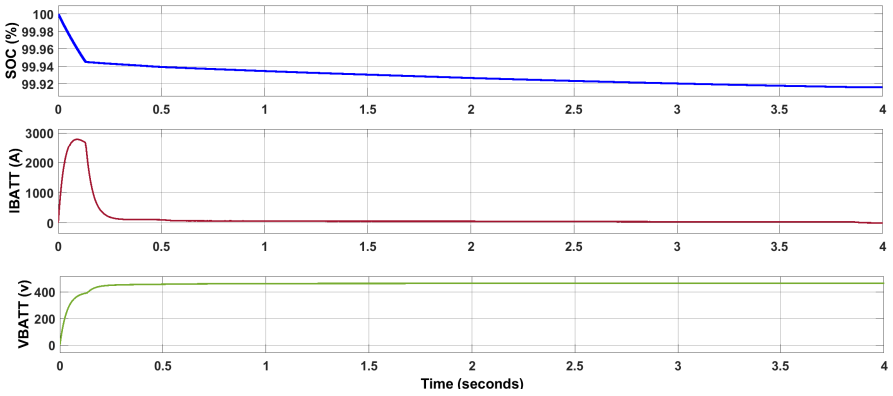

Figure 4-24: Battery parameters Voltage,Current and SOC%.

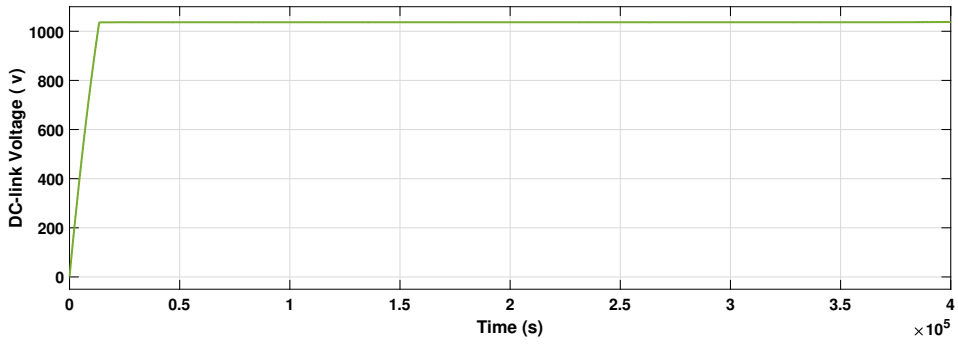

Figure 4-25: DC-link voltage of Inverting Buck Boost.

As it can be seen from the above results, in the motoring mode of operation, battery voltage reaches its fully charged value, along with an exponentially decreasing in battery's current and a decrease in SOC of the battery is observed. The DC-link voltage is rised up to 1040 v in a short

time response and maintains that value for the rest of the test duration. Hence, the Inverting Buck Boost is a suitable DC-DC converter for battery discharge mode in EVs.

4.4.2 Flyback converter

For many DC-DC converter applications, electrical isolation between the input and output ports is required for practical reasons such as safety. The flyback converter is a typical example. It is evolved from the buck boost converter by adding an isolation transformer used to store the energy instead of a single inductor.

Simulation results and Discussion

In order to evaluate the flyback converter for battery, simulation is conducted using a lithium battery with the corresponding parameters:rated voltage is 450V, rated capacity of 200 Ah and SOC set to 50%.

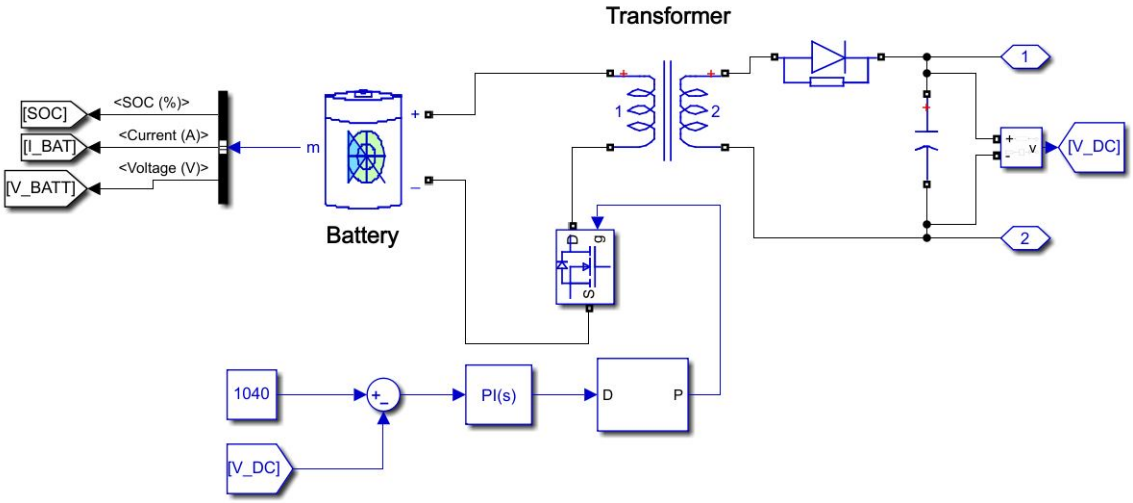

Figure 4-26: Simulink model of Flyback converter.

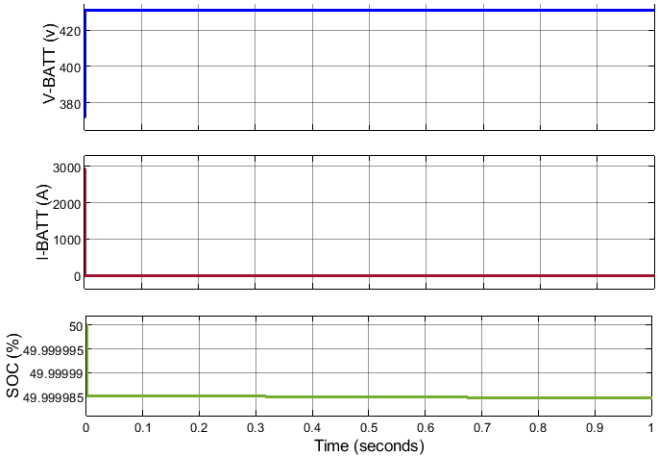

Figure 4-27: Battery parameters Voltage,Current and state of charge SOC%.

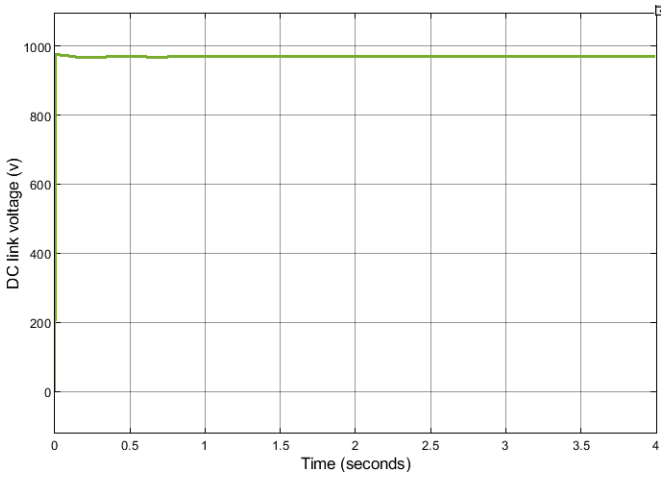

Figure 4-28: Dc-link voltage of Flyback converter.

From the simulation results, the discharging looks very fast which demonstrates that the flyback converter has a very fast response compared to the inverting buck boost type.

The above mentioned DC-DC converters provide current in a unidirectional way by having a single path for current to flow from the input source to the load. Thus, the use of a bidirectional DC-DC converter operating in the DC-link of an NSI fed two IMs devoted to EVs applications allows a suitable control of both motoring and regenerative braking operations.

4.5 Bidirectional DC-DC converter

In this section, a bidirectional DC–DC converter is connected between the battery and the NSI. Energy stored in batteries is transferred to the motor via DC–DC converter in the normal motoring operation. In this case, the DC–DC converter operates as a boost converter to boost battery terminal voltage to inverter's input voltage level. Consequently, during the regenerative mode of operation, DC–DC converter acts as a buck converter. The energy from the motor is transferred back to the source and can be used to charge the batteries[22]. The bidirectional half-bridge and interleaved buck boost topologies are investigated in this section.

4.5.1 Half-Bridge buck boost converter

To implement the battery charging and discharging process for EV applications, the half-bridge bidirectional DC-DC converter controlled by a fixed duty cycle is designated in this part. The forward braking is represented, where a negative torque with positive speed is applied(fourth quadrant in Figure1-7).

Simulation model and results

The topology of half-bridge bidirectional buck boost converter modeled in MATLAB/Simulink is shown in Figure4-29and Figure 4-30 followed by the results.

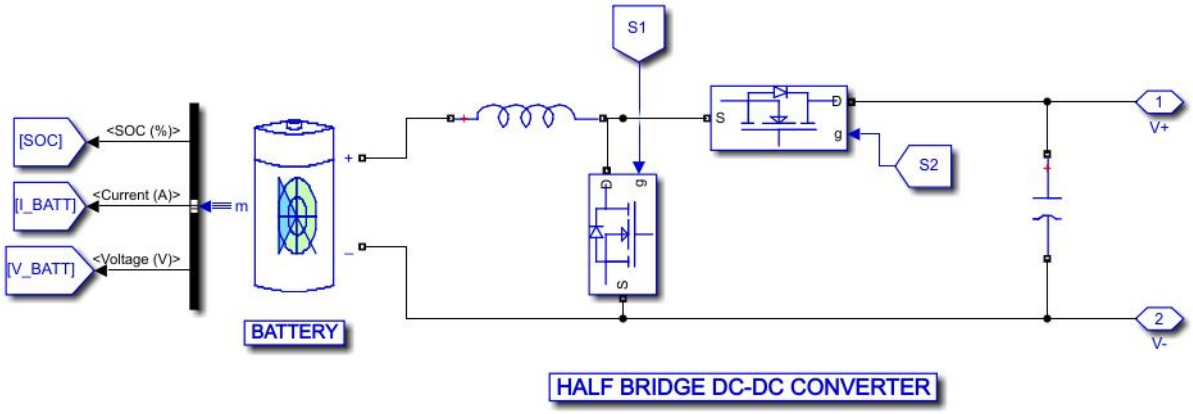

Figure 4-29: Half bridge DC-DC converter.

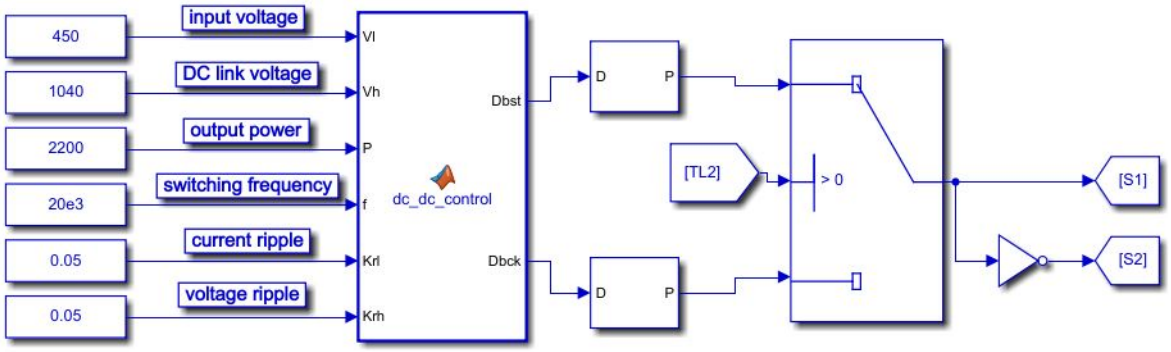

Figure 4-30: Control of half-bridge buck boost converter.

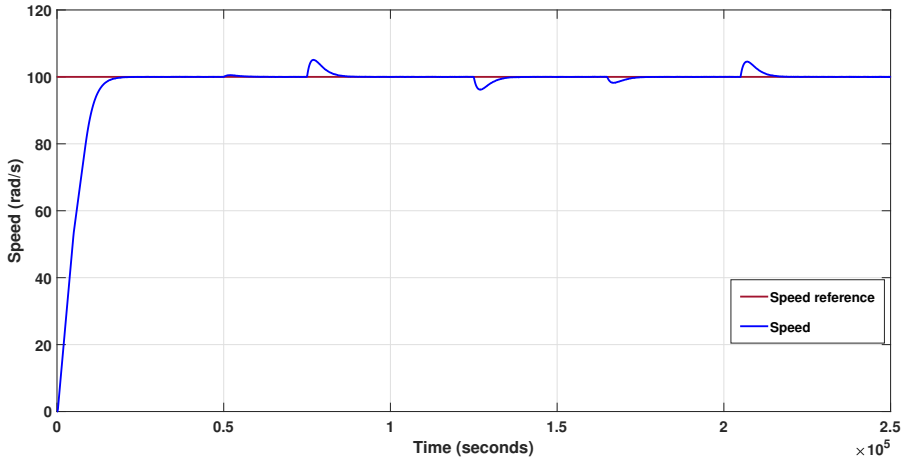

Figure 4-31: Rotor speed for the first motor.

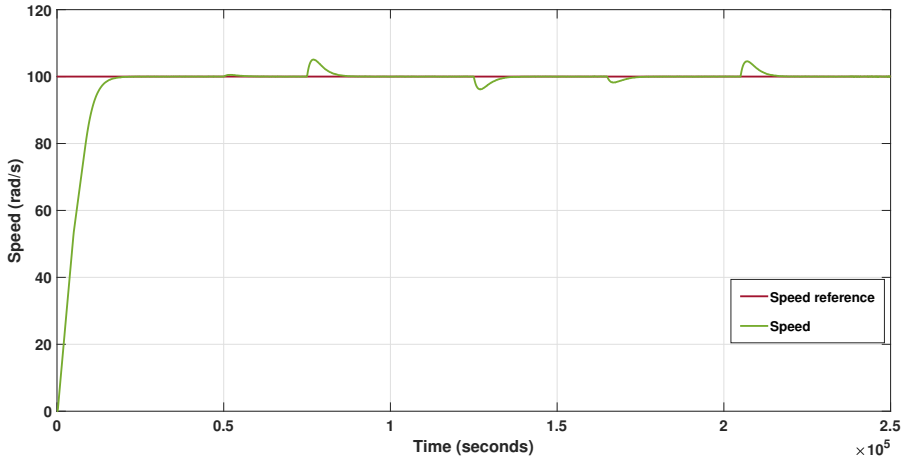

Figure 4-32: Rotor speed for the second motor.

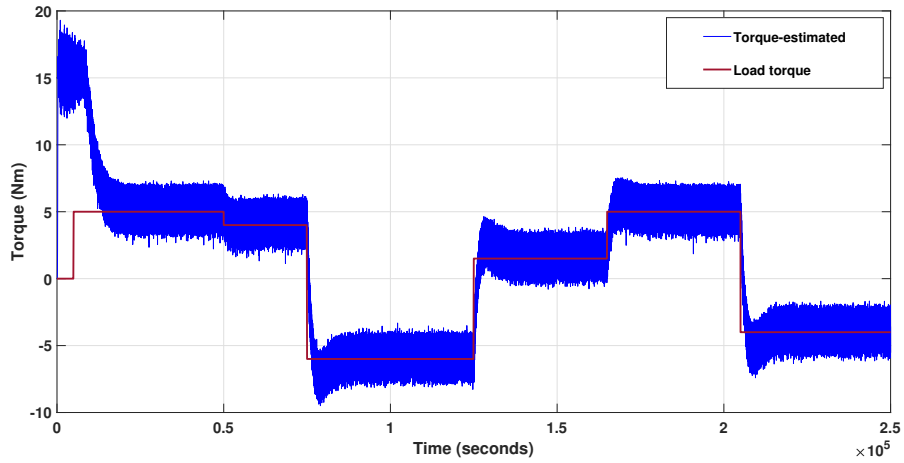

Figure 4-33: Electromagnetic torque for the first motor.

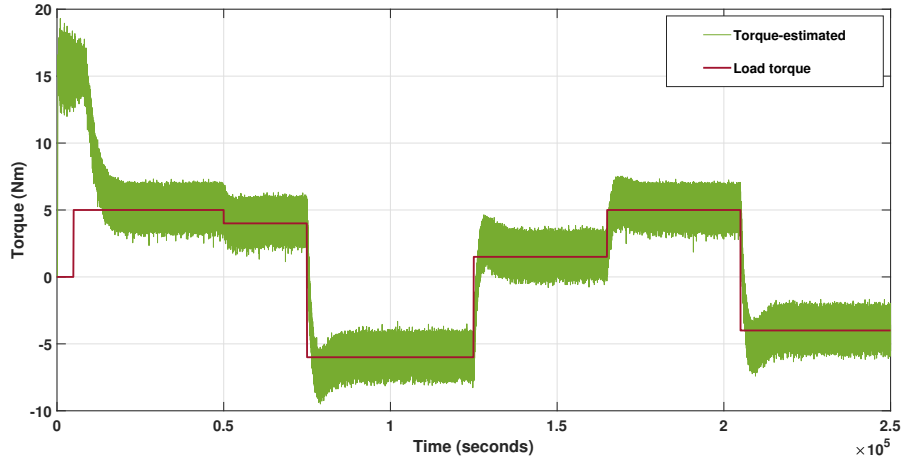

Figure 4-34: Electromagnetic torque for the second motor .

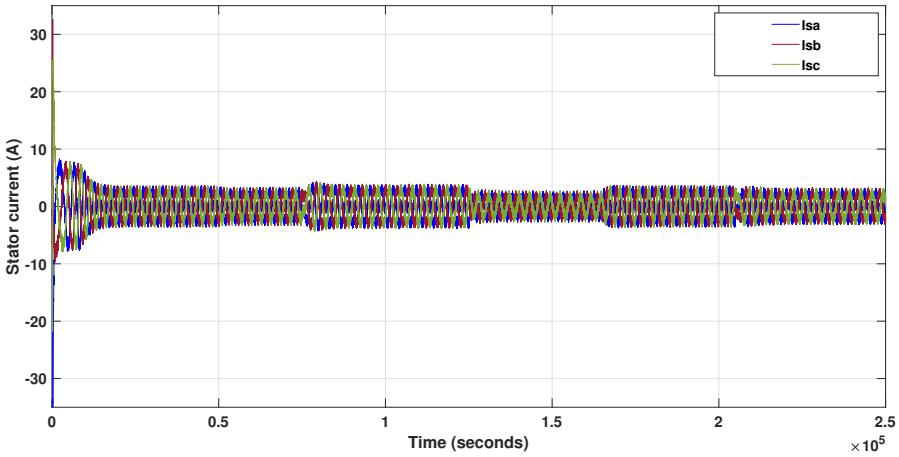

Figure 4-35: Stator current of the first motor.

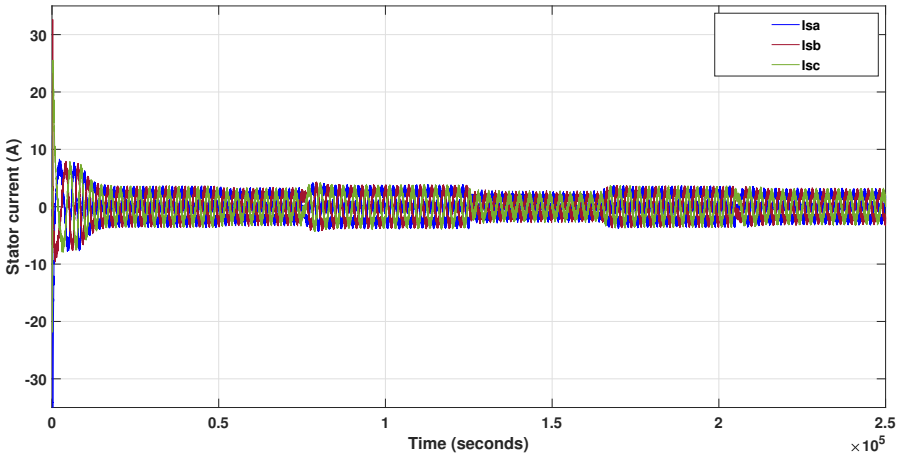

Figure 4-36: Stator current of the second motor.

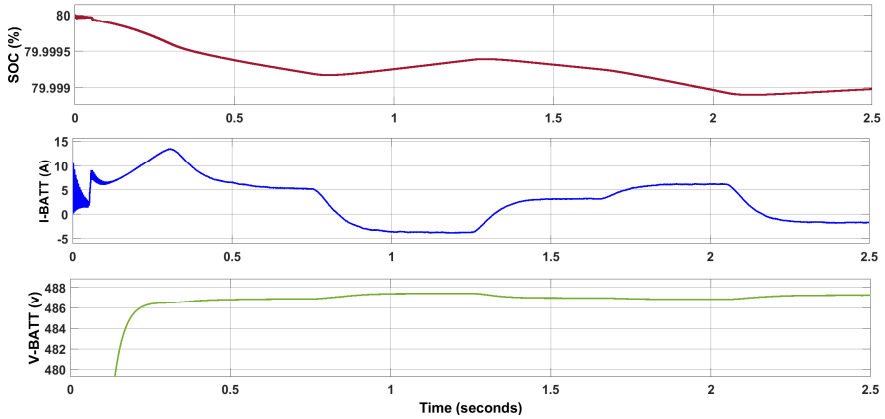

Figure 4-37: Battery parameters.

Discussion

As it can be noticed from both Figures 4-31 and 4-32, there is a good tracking of the speed during small rising time. Likewise, Figures 4-33 and 4-34 show that the actual torque pursue the requested reference. When the torque changes direction, a slight overshoot in the motors speed is noticed. The battery parameters are shown in Figure4-37. In motoring mode, the battery voltage is rised to the fully charged value, with the current being positive and decreasing in SOC is remarked. When the torque command's value switches from positive to negative, the battery's SOC increases and a rise in battery voltage is seen. The battery current also reverses its direction. A reverse in sequence occurs in stator current waveforms also can be seen clearly in Figures 4-35 and 4-36, signifying the battery is processing in the regenerative mode.

4.5.2 Closed loop control of interleaved buck boost converter

In interleaved buck boost Converter, two switches are connected in parallel. Using this configuration, the current can be divided through two switches. So the current stresses can be reduced. The closed loop control for the interleaved buck boost converter with PI controller is employed in this section.

- **PI controllers design**

  In boost mode, PI control of the DC-link voltage is used to maintain a constant DC-link voltage during driving operation. Battery voltage is controlled using another PI controller in buck mode to minimize voltage ripples. Ziegler-Nichols tunning method was used to design the PI controllers utilized in the feedback control for both operation modes.

Simulation model and results

The control system of the interleaved DC-DC converter in charge and discharge modes consists of two separate controllers, one for boost mode operation and the other for buck mode operation as illustrates in figure 4-39.

The selection of the aforementioned operations depends on the sign of the derivative of the speed reference curve and the direction of motion (moving the vehicle forward or backwards) which can be determined by the sign of the speed reference curve (positive speed reference for forward motion, negative speed reference for backwards motion). The speed and torque references are selected to simulate a real-world scenario where the driver increases the speed of the vehicle and decreases it while applying brakes. Simulation results are illustrated below.

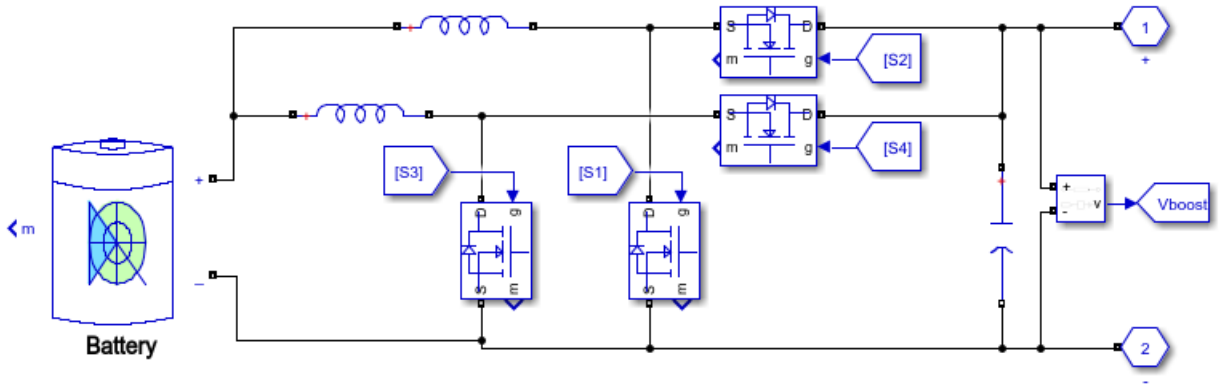

Figure 4-38: Interleaved DC-DC converter.

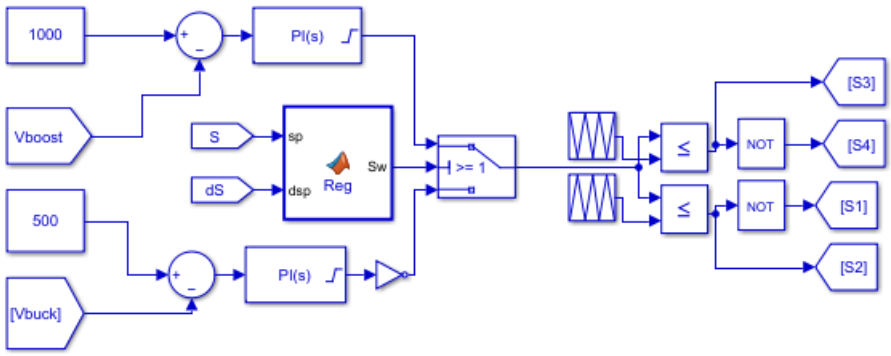

Figure 4-39: Control of the interleaved buck boost converter.

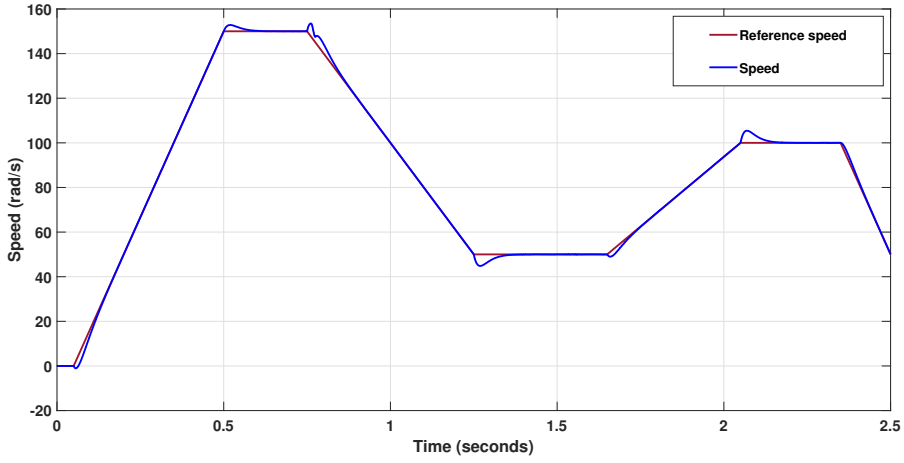

Figure 4-40: Rotor speed for the first motor.

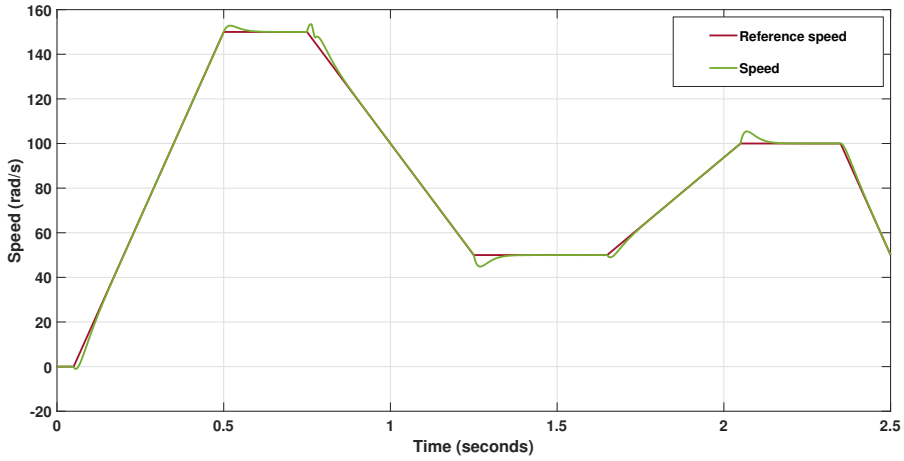

Figure 4-41: Rotor speed for the second motor.

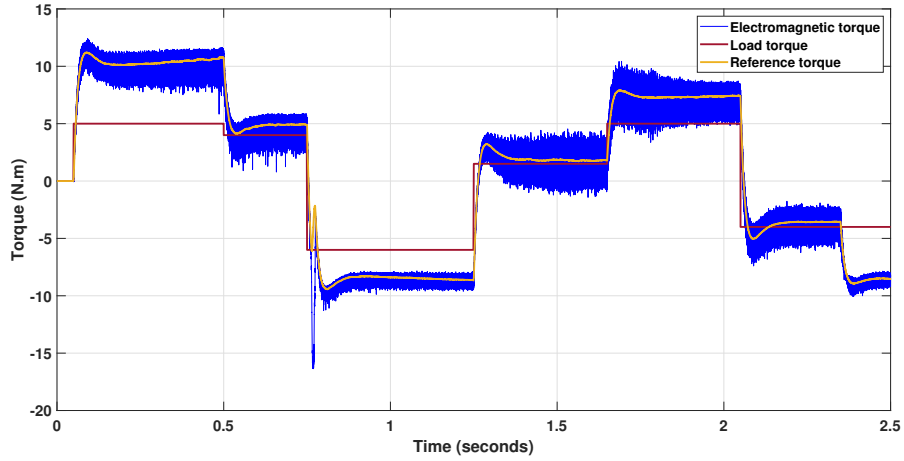

Figure 4-42: Electromagnetic torque for the first motor.

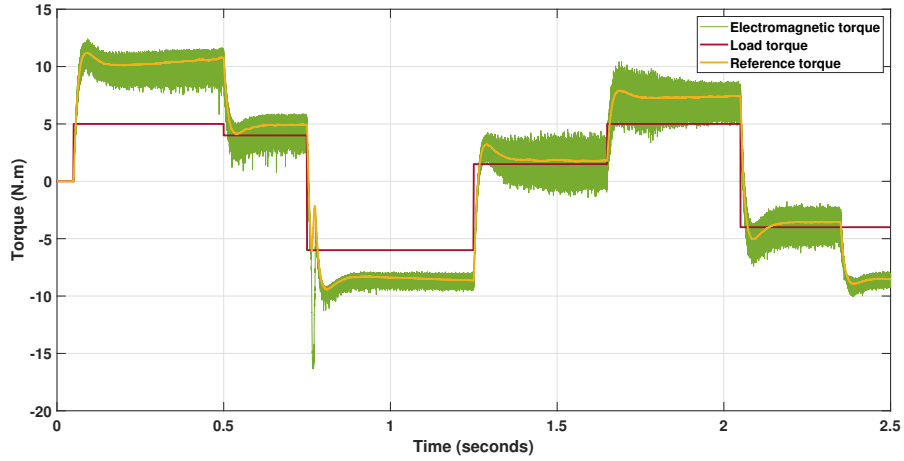

Figure 4-43: Electromagnetic torque for the second motor.

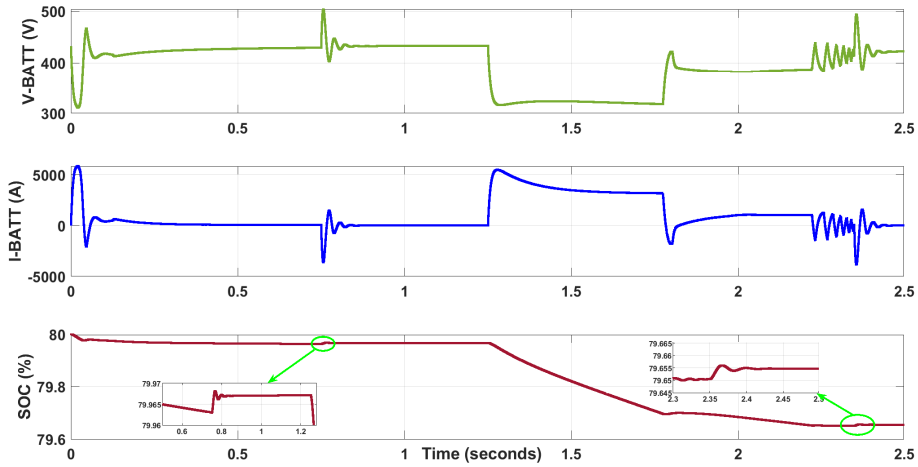

Figure 4-44: Battery parameters.

Discussion

In motoring mode (when speed of the vehicle is either increasing or constant), the battery voltage is kept to its fully charged voltage of around 440 v, the current is flowing from the battery to the load and the SOC is steadily decreasing indicating the battery is in discharge mode. The simulation results show precise tracking of speed as well as torque reference. When brakes are applied and speed starts to decrease, an increase in battery voltage is observed and the current is flowing from the load back to the battery and a small increase in SOC is noticed indicating the charge of the battery (regenerative mode). In transient state, the torque tracks its reference which differs from the load torque. In steady state, the torque tracks the load torque since it will be the same as reference torque.

4.6 Conclusion

In this chapter, DTC scheme with NSI based EVs were presented. A simple and effective algorithm is suggested to control the NSI using the DTC control scheme. Simulation results illustrate the independency in control and simultaneous supply of the two motors using the suggested algorithm. Additionally, Simulation of various DC-DC converters employed for battery charge/Discharge modes was held.Furthermore, the validity of controlling the EV traction chain and the viability of the aforementioned topologies were demonstrated.

General conclusion

The challenges of on-board applications, particularly in the field of electric vehicles, lie in the ability to design energy-efficient and space-saving systems at a lower cost. In this context, NSI, due to its compactness and the limited number of switches (limitation of switching losses), was proposed to drive the traction machines.

To effectively operate the two induction motors separately in this situation, while maintaining torque and stator flux ripples within acceptable bounds, DTC was suggested. Synchronism between the two motors, a simple and effective algorithm, was suggested to control the NSI using the DTC to ensure the stability for the vehicle when cornering or under slippery road conditions. Simulation studies have been carried out on Matlab/Simulink software, which proved the validity and efficiency of the DTC method with the proposed algorithm applied to the NSI driven two IMs.

For the power source of the EV, the low voltage (maximum reaches 450 v for Tesla model) provided by combination of series/parallel connected battery cells cannot supply two motors of 380 v. As a solution, a controlled DC-DC converter was used to boost the voltage. In motoring operation ,i.e. discharge mode, two types of unidirectional DC-DC converter were proposed for boosting the voltage at the required level in order to supply the NSI to motors. Comparative study was done between Inverting buck boost and flyback converter.

For energy saving in Electric Vehicles (EVs), high kinetic energy could be exploited by designing a regenerative braking control of traction machine. To achieve that, bidirectional DC-DC converter must replace the unidirectional to perform both modes alternatively depends on the actual condition. Two methods was tested ,fixed duty cycle and closed loop control. The discharging/charging of the battery at running/braking is validated by simulations.

Future work:

1-Improved control strategy based on model predictive control for EV application.

2-Energy management system for Hybrid electric vehicles (Fuel cell, Ultracapacitor).

3-Hardware implementation of DTC-NSI fed by battery via DC-DC converter.

Appendix

Table 4.1: Induction motor parameters

Machine's Power	$P = 1.1kw$
Stator resistance	$Rs = 6.75\ \Omega$
Roror resistane	$Rr = 6.21\ \Omega$
Stator inductance	$Ls = 0.5192H$
Rotor inductance	$Lr = 0.5192H$
Mutual inductance	M$sr = 0.4957H$
Number of pole pairs	$p = 2$
Friction coefficient	$f = 0.002$SI
The moment of inertia	$J = 0.01240kg.m^2$
Rated voltage	$Vs = 220/380V$

Bibliography

[1] K. T. Chau, *Electric vehicle machines and drives: design, analysis and application*. John Wiley & Sons, 2015.

[2] A. K. Sharma, A. Vyas, and P. Sharma, "Comparative study of dc-dc converter with different control techniques," *Available at SSRN 3808564*, 2021.

[3] L. M. Mansouri Houssam Eddine, *"Direct Torque Control of Two Induction Motors using the Nine-Switch inverter"*. 2021.

[4] F. Un-Noor, S. Padmanaban, L. Mihet-Popa, M. N. Mollah, and E. Hossain, "A comprehensive study of key electric vehicle (ev) components, technologies, challenges, impacts, and future direction of development," *Energies*, vol. 10, no. 8, p. 1217, 2017.

[5] M. Yildirim, M. Polat, and H. Kürüm, "A survey on comparison of electric motor types and drives used for electric vehicles," in *2014 16th International Power Electronics and Motion Control Conference and Exposition*, pp. 218–223, IEEE, 2014.

[6] J. A. Sanguesa, V. Torres-Sanz, P. Garrido, F. J. Martinez, and J. M. Marquez-Barja, "A review on electric vehicles: Technologies and challenges," *Smart Cities*, vol. 4, no. 1, pp. 372–404, 2021.

[7] M. Ismail and A. Hichem, *"La commande en vitesse d'un véhicule électrique"*. 2019.

[8] M. Al Sakka, J. Van Mierlo, H. Gualous, and U. Brussel, "Dc/dc converters for electric vehicles," *Electric Vehicles-Modelling and Simulations*, vol. 100, p. 466, 2011.

[9] A. J. Luan, "Bi-directional flyback dc-dc converter for battery system of the dc house project," 2013.

[10] I. Azizi and H. Radjeai, "A bidirectional dc-dc converter fed dc motor for electric vehicle application," in *2015 4th International Conference on Electrical Engineering (ICEE)*, pp. 1–5, IEEE, 2015.

[11] Z. Wang, J. Zhang, P. Liu, C. Qu, and X. Li, "Driving cycle construction for electric vehicles based on markov chain and monte carlo method: A case study in beijing," *Energy Procedia*, vol. 158, pp. 2494–2499, 2019.

[12] S. krishnan, "What are driving cycles and how to develop one for electric vehicle simulation?," 2018.

[13] T. Kominami and Y. Fujimoto, "A novel nine-switch inverter for independent control of two three-phase loads," in *2007 IEEE Industry applications annual meeting*, pp. 2346–2350, IEEE, 2007.

[14] D. J. Rhees, "Electricity-" the greatest of all doctors": An introduction to" high frequency oscillators for electro-therapeutic and other purposes"," *Proceedings of the IEEE*, vol. 87, no. 7, pp. 1277–1281, 1999.

[15] A. Ammar, *Improvement of Direct Torque Control Performances for Asynchronous Machine Using Non-Linear Techniques*. PhD thesis, Thesis, University Mohamed Khider, Biskra, Algeria, 2017.

[16] K. Brun and R. Kurz, *Compression machinery for oil and gas*. Gulf Professional Publishing, 2018.

[17] F. Gao, L. Zhang, D. Li, P. C. Loh, Y. Tang, and H. Gao, "Optimal pulsewidth modulation of nine-switch converter," *IEEE Transactions on Power Electronics*, vol. 25, no. 9, pp. 2331–2343, 2010.

[18] D. Abdelghani and A. Boumediene, "Independent control of two induction motors fed by the nine-switch inverter for use in ev applications," *Journal of Engineering Science and Technology*, vol. 14, no. 5, pp. 2991–3006, 2019.

[19] H. Abu-Rub, A. Iqbal, and J. Guzinski, *High performance control of AC drives with Matlab/Simulink*. John Wiley & Sons, 2021.

[20] Z. Alnasir and A. Almarhoon, "Design of direct torque controller of induction motor (dtc)," *International Journal of Engineering and Technology (IJET)*, vol. 4, no. 2, pp. 54–70, 2012.

[21] J.-W. Kang and S.-K. Sul, "Analysis and prediction of inverter switching frequency in direct torque control of induction machine based on hysteresis bands and machine parameters," *IEEE Transactions on Industrial Electronics*, vol. 48, no. 3, pp. 545–553, 2001.

[22] T. Sharma and A. Bhattacharya, "Performance analysis of encoderless dtc of ipmsm for wide operating range," *Arabian Journal for Science and Engineering*, vol. 45, no. 8, pp. 6501–6515, 2020.